Atmos. Chem. Phys. Discuss., 12, 26047–26097, 2012
www.atmos-chem-phys-discuss.net/12/26047/2012/
doi:10.5194/acpd-12-26047-2012

Atmospheric Chemistry and Physics Discussions

Tropospheric ozone changes, radiative forcing and attribution to emissions in the Atmospheric Chemistry and Climate Model Inter-comparison Project (ACCMIP)

D. S. Stevenson[1], P. J. Young[2,3], V. Naik[4], J.-F. Lamarque[5], D. T. Shindell[6], A. Voulgarakis[7], R. B. Skeie[8], S. B. Dalsoren[8], G. Myhre[8], T. K. Berntsen[8], G. A. Folberth[9], S. T. Rumbold[9], W. J. Collins[9], I. A. MacKenzie[1], R. M. Doherty[1], G. Zeng[10], T. P. C. van Noije[11], A. Strunk[11], D. Bergmann[12], P. Cameron-Smith[12], D. A. Plummer[13], S. A. Strode[14], L. Horowitz[15], Y. H. Lee[6], S. Szopa[16], K. Sudo[17], T. Nagashima[18], B. Josse[19], I. Cionni[20], M. Righi[21], V. Eyring[21], A. Conley[5], K. W. Bowman[22], and O. Wild[23]

[1]School of GeoSciences, The University of Edinburgh, Edinburgh, UK
[2]Chemical Sciences Division, NOAA Earth System Research Laboratory, Boulder, Colorado, USA
[3]Cooperative Institute for Research in Environmental Sciences, University of Colorado, Boulder, Colorado, USA
[4]UCAR/NOAA Geophysical Fluid Dynamics Laboratory, Princeton, New Jersey, USA

[5]National Center for Atmospheric Research, Boulder, Colorado, USA
[6]NASA Goddard Institute for Space Studies and Columbia Earth Institute, New York, NY, USA
[7]Department of Physics, Imperial College London, London, UK
[8]CICERO, Center for International Climate and Environmental Research-Oslo, Oslo, Norway
[9]Met Office Hadley Centre, Exeter, UK
[10]National Institute of Water and Atmospheric Research, Lauder, New Zealand
[11]Royal Netherlands Meteorological Institute, De Bilt, The Netherlands
[12]Lawrence Livermore National Laboratory, Livermore, California, USA
[13]Canadian Centre for Climate Modeling and Analysis, Environment Canada, Victoria, British Columbia, Canada
[14]NASA Goddard Space Flight Centre, Greenbelt, Maryland, USA and Universities Space Research Association, Columbia, MD, USA
[15]NOAA Geophysical Fluid Dynamics Laboratory, Princeton, New Jersey, USA
[16]Laboratoire des Sciences du Climat et de l'Environment, Gif-sur-Yvette, France
[17]Department of Earth and Environmental Science, Graduate School of Environmental Studies, Nagoya University, Nagoya, Japan
[18]National Institute for Environmental Studies, Tsukuba-shi, Ibaraki, Japan
[19]GAME/CNRM, Météo-France, CNRS – Centre National de Recherches Météorologiques, Toulouse, France
[20]Agenzia Nazionale per le Nuove Tecnologie, l'energia e lo Sviluppo Economico Sostenibile (ENEA), Bologna, Italy
[21]Deutsches Zentrum für Luft- und Raumfahrt (DLR), Institut für Physik der Atmosphäre, Oberpfaffenhofen, Germany
[22]NASA Jet Propulsion Laboratory, Pasadena, California, USA
[23]Lancaster Environment Centre, University of Lancaster, Lancaster, UK

Received: 31 July 2012 – Accepted: 24 September 2012 – Published: 4 October 2012

Correspondence to: D. S. Stevenson (david.s.stevenson@ed.ac.uk)

Published by Copernicus Publications on behalf of the European Geosciences Union.

ACPD
12, 26047–26097, 2012

Abstract

Ozone (O_3) from 17 atmospheric chemistry models taking part in the Atmospheric Chemistry and Climate Model Intercomparison Project (ACCMIP) has been used to calculate tropospheric ozone radiative forcings (RFs). We calculate a value for the pre-industrial (1750) to present-day (2010) tropospheric ozone RF of 0.40 $W m^{-2}$. The model range of pre-industrial to present-day changes in O_3 produces a spread (±1 standard deviation) in RFs of ±17 %. Three different radiation schemes were used – we find differences in RFs between schemes (for the same ozone fields) of ±10 %. Applying two different tropopause definitions gives differences in RFs of ±3 %. Given additional (unquantified) uncertainties associated with emissions, climate-chemistry interactions and land-use change, we estimate an overall uncertainty of ±30 % for the tropospheric ozone RF. Experiments carried out by a subset of six models attribute tropospheric ozone RF to increased emissions of methane (47 %), nitrogen oxides (29 %), carbon monoxide (15 %) and non-methane volatile organic compounds (9 %); earlier studies attributed more of the tropospheric ozone RF to methane and less to nitrogen oxides. Normalising RFs to changes in tropospheric column ozone, we find a global mean normalised RF of 0.042 $W m^{-2} DU^{-1}$, a value similar to previous work. Using normalised RFs and future tropospheric column ozone projections we calculate future tropospheric ozone RFs ($W m^{-2}$; relative to 1850 – add 0.04 $W m^{-2}$ to make relative to 1750) for the Representative Concentration Pathways in 2030 (2100) of: RCP2.6: 0.31 (0.16); RCP4.5: 0.38 (0.26); RCP6.0: 0.33 (0.24); and RCP8.5: 0.42 (0.56). Models show some coherent responses of ozone to climate change: decreases in the tropical lower troposphere, associated with increases in water vapour; and increases in the sub-tropical to mid-latitude upper troposphere, associated with increases in lightning and stratosphere-to-troposphere transport.

ACPD

12, 26047–26097, 2012

1 Introduction

While estimates of many aspects of Earth's past atmospheric composition can be derived from analyses of air trapped in bubbles during ice formation (Wolff, 2011), the greenhouse gas ozone (O_3) is too reactive to be preserved in this way. Direct measurements of tropospheric ozone concentrations prior to the 1970s are also extremely limited (Volz and Kley, 1988; Staehelin et al., 1994), and most early measurements used relatively crude techniques, such as Schönbein papers (Rubin, 2001), that are subject to contamination from compounds other than ozone (Pavelin et al., 1999). Only in the last few decades have observation networks and analytical methods developed sufficiently to allow a global picture of ozone's distribution in the troposphere to emerge (Fishman et al., 1990; Logan, 1999; Oltmans et al., 2006; Thouret et al., 2006). Despite this paucity of early observations, tropospheric ozone is thought to have increased substantially since the pre-industrial era; this is largely based on model studies. Ozone photochemistry in the troposphere is relatively well understood (Crutzen, 1974; Derwent et al., 1996), and anthropogenic (including biomass burning) emissions of ozone precursors (methane, CH_4; nitrogen oxides, NO_x; carbon monoxide, CO; and non-methane volatile organic compounds, NMVOCs) have changed (generally risen) dramatically since pre-industrial times (Lamarque et al., 2010). Increasingly sophisticated models of atmospheric chemistry, driven by emission estimates, and sometimes coupled to climate models, have been used to simulate the rise of ozone since industrialisation (Hough and Derwent, 1990; Crutzen and Zimmerman, 1991; Berntsen et al., 1997; Wang and Jacob, 1998; Gauss et al., 2006).

Although increases in anthropogenic precursor emissions have been the main driver of ozone change, several other factors may also have contributed. Natural sources of precursor emissions (e.g. wetland CH_4, soil and lightning NO_x, biogenic NMVOCs) show significant variability and have probably also changed since the pre-industrial era, but these changes are highly uncertain (Arneth et al., 2010). Downwards transport of ozone from the stratosphere is also an important source of tropospheric ozone

ACPD
12, 26047–26097, 2012

(Stohl et al., 2003; Hsu and Prather, 2009); this source may have been affected by stratospheric ozone depletion, and is forecast to change in the future, via ozone recovery and acceleration of the Brewer-Dobson circulation (Hegglin and Shepherd, 2009; Zeng et al., 2010; SPARC-CCMVal, 2010), although attempts to diagnose circulation changes from observations have given ambiguous results (Engel et al., 2009; Lin et al., 2009; Ray et al., 2010; Young et al., 2012b). Ozone's removal, via chemical, physical and biological processes is also subject to variability and change. Increases in absolute humidity (driven by warming), changes in ozone's distribution, and changes in OH and HO_2 (HO_x), have all tended to increase chemical destruction of ozone (Johnson et al., 2001; Stevenson et al., 2006; Isaksen et al., 2009). Dry deposition of ozone at the surface, and to vegetation in particular, has been influenced by land-use change, but also by changes in climate and CO_2 abundance (Sanderson et al., 2007; Sitch et al., 2007; Fowler et al., 2009; Andersson and Engardt, 2010; Ganzeveld et al., 2010; Wu et al., 2012). Fluctuations in these natural sources and sinks are driven by climate variability; climate change and land-use change may also have contributed towards long-term trends in ozone.

Ozone is a radiatively active gas, and interacts with both solar (shortwave, SW) and terrestrial (longwave, LW) radiation, meaning that changes in its atmospheric distribution affect both upwards and downwards fluxes of radiation. Increases in ozone have consequently contributed to climate warming (e.g. Lacis et al., 1990). We use the concept of radiative forcing (RF) (e.g. as defined by Forster et al., 2007) to quantify the impacts of tropospheric ozone changes on Earth's radiation budget since the pre-industrial period. Specifically, in this paper we follow the Intergovernmental Panel on Climate Change (IPCC) and use stratospherically-adjusted RFs at the tropopause (Forster et al., 2007). Previous estimates of the tropospheric ozone RF (e.g. Gauss et al., 2006) span the range 0.25–0.65 $W m^{-2}$, with a central value of 0.35 $W m^{-2}$ for the RF from 1750–2005 (Forster et al., 2007). Skeie et al. (2011) recently estimated a value of 0.44 $W m^{-2}$, with an uncertainty of ±30 %, using one of the models we also use in this study. Cionni et al. (2011) calculated ozone RFs for the IGAC/SPARC

ACPD
12, 26047–26097, 2012

(International Global Atmospheric Chemistry/Stratospheric Processes and their Role in Climate) ozone database, and found a tropospheric ozone RF (1850s–2000s) of 0.23 $W m^{-2}$, using an earlier version of the main radiation scheme used here. Using an updated version of this radiation scheme with exactly the same ozone fields we find an equivalent, and presumed more accurate, value of 0.32 $W m^{-2}$. The tropospheric part of the IGAC/SPARC ozone database was constructed from early ACCMIP integrations from two of the 17 models used here (GISS-E2-R and NCAR-CAM3.5). Through the use of additional models, we consider the multi-model mean results presented here to be a more robust estimate of atmospheric composition change than the IGAC/SPARC database.

Because ozone is a secondary pollutant (i.e. it is not directly emitted), it is useful to understand how emissions of its precursors have driven up its concentration. Model experiments carried out by Shindell et al. (2005, 2009) attributed pre-industrial to present-day ozone changes to increases in CH_4, NO_x, CO and NMVOC emissions, finding that methane emissions were responsible for most of the ozone change. These emissions also influence the oxidising capacity of the atmosphere in general, and affect a range of radiatively active species beyond ozone, including methane and secondary aerosols (Shindell et al., 2009).

In this paper, we present results from global models participating in the Atmospheric Chemistry and Climate Model Intercomparison Project (ACCMIP; see www.giss.nasa.gov/projects/accmip). Within ACCMIP, multiple models simulated atmospheric composition between 1850–2100. Lamarque et al. (2012) give an overview of ACCMIP and present detailed descriptions of the participating models and model simulations. Shindell et al. (2012) describe total radiative forcings, particularly those from aerosols; Lee et al. (2012) further focus on black carbon aerosol. Young et al. (2012a) describe the ozone results in detail, including a range of comparisons with observations; Bowman et al. (2012) focus on comparisons with measurements from TES (Tropospheric Emission Spectrometer). Voulgarakis et al. (2012) document the evolution of the oxidising capacity of the atmosphere, especially OH and its impact on methane lifetime.

ACPD
12, 26047–26097, 2012

This paper looks in detail at tropospheric ozone RFs from the ACCMIP simulations. In Sect. 2, the models used and the experiments they performed are described. Results of simulated ozone and resulting radiative forcings are presented in Sect. 3; these are discussed and conclusions are drawn in Sect. 4. For conciseness, the main text focusses on generalised results (often presented as the multi-model mean) and specific results from individual models are predominantly presented in the Supplement.

2 Methods

2.1 Models employed

Results from 17 different models are analysed here (Table 1). Detailed model descriptions are provided in Lamarque et al. (2012); for model Q (TM5) see: Huijnen et al. (2010) and Von Hardenberg et al. (2012). All are global atmospheric chemistry models, and most are coupled to climate models, which provide the driving meteorological fields. Climate model output of sea-surface temperatures and sea-ice concentrations (SST/SIC) from prior CMIP5 runs typically provide the lower boundary conditions; well-mixed atmospheric greenhouse gas concentrations are also specified. Three models (B, Q and M) are chemistry-transport models, driven by offline meteorological analyses (B and Q) or offline output from a climate model (M). Additionally, models B and Q provide only a single year's output for each experiment and were run with the same meteorology in each case. In all other models, the chemistry module is embedded within a general circulation model. With the exception of models O and P, the calculated chemical fields are used in the climate model's radiation scheme; i.e. they are fully coupled chemistry-climate models (CCM). Models G and H are two versions of GISS-E2-R, but set up in different ways: G has a fully interactive coupled ocean (the only model with this) whilst H uses SST/SIC from GISS-E2-R but also includes a more sophisticated aerosol microphysics scheme instead of the simpler mass-based scheme used in G. Models I and J are two versions of HadGEM2: I uses a relatively

ACPD
12, 26047–26097, 2012

simple tropospheric chemistry scheme, whereas J has a more detailed scheme with several hydrocarbons. Several models (C, D, E, F, G, H, L, M, and N) include detailed stratospheric chemistry schemes; tropospheric schemes range from simple methane oxidation (C) through models with a basic representation of NMVOCs (A, G, H, I, and P) to those with more detailed hydrocarbon schemes (B, D, E, F, J, K, L, M, N, O and Q). In addition, some models include interactions between aerosols and gas-phase chemistry (B, F, G, H, I, J, K, L, N, and Q).

Models without detailed stratospheric chemistry handled their upper levels in a variety of different ways. Model A simulated simulated stratospheric ozone using the LINOZ scheme (McLinden et al., 2000). Model B used monthly model climatological values of ozone and nitrogen species, except in the three lowermost layers of the stratosphere (approximately 2.5 km) where the tropospheric chemistry scheme is applied to account for photochemical ozone production (Skeie et al., 2011). Models I, J, K, O, P and Q all used the IGAC/SPARC ozone database (Cionni et al., 2011) to prescribe ozone in the stratosphere. In models I and J, ozone is overwritten in all model levels which are 3 levels (approximately 3–4 km) above the tropopause. Model O used the ozone fields together with vertical winds, to calculate a vertical ozone flux at 100 hPa, added as an ozone source at these levels in regions of descent. Model P prescribed ozone at pressures below 100 hPa between 50° S–50° N and pressures below 150 hPa poleward of 50°, and model Q at pressures below 45 hPa between 30° S–30° N and pressures below 90 hPa poleward of 30°.

Some models allowed natural emissions of ozone precursors to vary with climate; others fixed these sources (Table 2).

2.2 Model simulations

The main experiments analysed here are multi-annual simulations for the 1850s and the 2000s. Every model performed these experiments. Table 1 shows the model run length for each experiment: typically 10 yr, but in a few cases longer or shorter. Model G ran five 10-yr ensemble members. In most cases, models simulated climates of

ACPD
12, 26047–26097, 2012

the 1850s and 2000s, typically by specifying SST/SIC fields (typically decadally averaged from prior coupled ocean–atmosphere climate simulations) and setting well-mixed greenhouse gas concentrations at appropriate levels. Models B, J and Q ran with the same climate in the 1850s as in their 2000s runs, so only assess how emissions have changed composition; single year experiments are thus not unreasonable in these cases.

All models used anthropogenic emissions (including biomass burning emissions, which are partly anthropogenic and partly natural) from Lamarque et al. (2010). This harmonisation of all models to the same source of emissions removes a potentially large source of inter-model difference (cf. Gauss et al., 2006). However, as each model did not run exactly the same years to represent the 1850s and 2000s (see Table 1), and models used a range of values for natural emissions (Table 2) there are still some differences between models in the magnitude of the applied change in emissions (see Young et al., 2012a, Fig. 1). Note that the model years specified in Table 1 refer to nominal years for the driving climate, but not for the emissions. These differences are added to by different chemistry schemes and decisions within each model of how to partition NMVOC emissions between individual species and/or to emit directly as CO emissions.

Most models ran with prescribed methane concentrations of around 791 ppbv (1850s) and 1751 ppbv (2000s) (Prinn et al., 2000; Meinshausen et al., 2011). One model (K) ran with methane emissions for the historical period, allowing methane concentrations to evolve.

Six of the models (Table 1) ran a series of attribution experiments, based on the 2000s simulations. In these, specific drivers of ozone change (anthropogenic emissions of NO_x, CO, NMVOCs, and CH_4 concentrations) were individually reduced to 1850s levels. These experiments are closely related to previous studies with the GISS model (Shindell et al., 2005, 2009), and allow us to attribute methane and ozone radiative forcings since the 1850s to these individual drivers, although we do not consider how the individual drivers interact.

ACPD
12, 26047–26097, 2012

A subset of ten models (Table 1) ran experiments where they fixed emissions at 2000s levels, but applied an 1850s climate. These simulations allow us to investigate how climate change has contributed to the ozone change since the 1850s. Most of these models also ran equivalent experiments for future climates.

Finally, most models (Table 1) ran additional historical and future simulations, using harmonized emissions from the Representative Concentration Pathway (RCP) scenarios, and prescribing methane concentrations (Meinshausen et al., 2011). Models K and G ran with methane emissions in the future, allowing methane concentrations to freely evolve. Ozone fields from these experiments are presented in detail by Young et al. (2012a) – here we use future tropospheric column ozone changes in conjunction with normalised radiative forcings ($mW\,m^{-2}\,DU^{-1}$) to estimate future tropospheric ozone radiative forcings.

2.3 Radiative forcing calculations

Ozone fields were inserted into an offline version of the Edwards and Slingo (1996) radiation scheme, updated and described by Walters et al. (2011) (their Sect. 3.2). The scheme includes gaseous absorption in six bands in the SW and nine bands in the LW. The treatment of ozone absorption is as described by Zhong et al. (2008). The RF calculations use an updated version of the radiation code compared with those presented by Cionni et al. (2011), and it is found that these updates make substantial differences in the values. The updated calculations presented here supersede the RF calculations from Cionni et al. (2011) that were calculated with the older version of the radiation scheme and from two rather than 17 models in this study.

The offline code was set up so that all input fields except ozone remained fixed (at present-day values) – thus differences between two runs of the radiation code with different ozone yield the changes in fluxes of radiation due to ozone change alone. Monthly mean ozone fields were interpolated from each model to a common resolution: 5° longitude by 5° latitude, and 64 hybrid vertical levels up to 0.01 hPa. The vertical levels were chosen to be compatible with the base climatological fields (temperature,

ACPD
12, 26047–26097, 2012

humidity, cloud fields), taken from a present-day simulation of the HadAM3 model (Pope et al., 2000; Tian and Chipperfield, 2005). Values for cloud particle effective radii were taken from the GRAPE (Global Retrieval of ATSR (Along Track Scanning Radiometer) cloud Parameters and Evaluation) dataset (Sayer et al., 2011).

To calculate an ozone radiative forcing, the code is applied as follows. A base calculation of radiation fluxes is performed, using multi-annually averaged monthly ozone data from the 1850s, for each column of the model atmosphere. The radiation calculation is then repeated, keeping everything the same, but using a different ozone field (e.g. from the 2000s). The change in net radiation at the tropopause between these two calculations gives the instantaneous radiative forcing. In this study, we only consider changes in tropospheric ozone, by overwriting ozone fields above the tropopause with climatological values taken from Cionni et al. (2011) (up to 1 hPa) and values from Li and Shine (1995) at higher altitudes.

By changing the ozone field, heating rates in the stratosphere will have changed. If such a change were to happen in the real atmosphere, stratospheric temperatures would respond quickly (days to months, e.g. Hansen et al., 1997) – much more quickly than the surface-troposphere system, which will adjust on multiannual timescales. A better estimate of the long-term forcing on the surface climate takes into account this short-term response of stratospheric temperatures (Forster et al., 2007). Stratospheric temperature adjustment was achieved by first calculating stratospheric heating rates for the base atmosphere. The stratosphere was assumed to be in thermal equilibrium, i.e. with dynamical heating exactly balancing the radiative heating. Furthermore, the dynamics were assumed to remain constant following a perturbation to ozone. Hence to maintain equilibrium, radiative heating rates must also remain unchanged. To achieve this, stratospheric temperatures were iteratively adjusted in the perturbed case, until stratospheric radiative heating rates returned to their base values. This procedure is called the fixed dynamical heating approximation (Ramanathan and Dickinson, 1979). Here we report annual mean forcings at the tropopause, after stratospheric temperature adjustment.

ACPD
12, 26047–26097, 2012

We compare calculations with the Edwards-Slingo radiation scheme to results from similar schemes from the University of Oslo and the National Center for Atmospheric Research (NCAR). The Oslo radiative transfer calculations are performed with a broad band longwave scheme (Myhre and Stordal, 1997) and a model using the discrete ordinate method (Stamnes et al., 1988) for the shortwave calculations (see further description in Myhre et al., 2011). Meteorological data from ECMWF (European Centre for Medium-range Weather Forecasting) are used and stratospheric temperature adjustment is included. The NCAR calculations used the NCAR Community Climate System Model 4 offline radiative transfer model, also allowing stratospheric temperatures to adjust. Net LW and SW all-sky fluxes at the tropopause (based on a climatology of tropopause pressure from the NCAR/NCEP reanalyses) were computed using the same conditions for all parameters except for the ozone distribution.

3 Results

3.1 Pre-industrial (1850s) and present-day (2000s) simulations

3.1.1 Core ACCMIP experiments

Ozone distributions and changes

Figure 1 shows the multi-model mean (MMM) annual zonal mean (AZM) ozone for the 1850s and 2000s. All models are included in the MMM, with equal weighting. In the Supplement, Fig. S1 shows AZM ozone (ppbv) for the 1850s and 2000s for all 17 models. Figure 2 shows maps of MMM tropospheric column ozone (DU) for the 1850s and 2000s. Figure S2 is the equivalent for all 17 models. In these figures, we use the same monthly zonal mean climatological tropopause (hereafter referred to as MASKZMT) for all models, based on the 2 PVU definition applied to present-day NCEP/NCAR reanalysis data (Cionni et al., 2011). We also calculate ozone changes and radiative

ACPD
12, 26047–26097, 2012

forcing results using a different tropopause definition (1850s O_3=150 ppbv; hereafter referred to as MASK150; as used in Young et al., 2012a) to test how sensitive results are to this choice. The MASKZMT tropopause is the same for all models (and all time slices); the MASK150 tropopause is different for each model, but the same for all time slices of a given model. Table 3 compares global mean tropospheric column ozone changes using both definitions for all models. Evaluation of simulated present-day ozone fields against a variety of observational data sets can be found elsewhere (Young et al., 2012a). Overall, present-day distributions are similar to those presented by Stevenson et al. (2006) from the ACCENT PhotoComp model intercomparison. Figure 3 shows the MMM change (2000s–1850s) in AZM ozone (ppbv) and tropospheric column ozone (DU) for MASKZMT. Figure S3 is the equivalent for all 17 models. Ozone generally increases throughout the troposphere, most strongly in the Northern Hemisphere sub-tropical upper troposphere. This mainly reflects the industrialised latitudes where emissions are concentrated, and the fact that the ozone lifetime is longer in the upper troposphere. Decreases in ozone are seen in the high latitudes of the Southern Hemisphere (SH) in many models (Figs. 3 and S3). This reflects the present-day ozone depletion (relative to the 1850s) of air transported downwards from the stratosphere, and is especially pronounced in models M, G and H. This effect is strong enough in several models to produce decreases in tropospheric column ozone in high SH latitudes (Fig. S3).

Ozone radiative forcings

Figure 4 shows maps of the multi-model annual mean radiative forcing ($mW\,m^{-2}$) in the total (SW + LW), SW, and LW, using MASKZMT. Table 3 and Fig. S4a show the total RFs for all 17 models; Fig. S4b shows the equivalent plot to Fig. 4 for ozone from the IGAC/SPARC database (Cionni et al., 2011). The LW RF peaks in regions where large ozone changes coincide with hot surface temperatures and cold tropopause temperatures (e.g. over the Sahara and Middle East). The SW RF peaks where large ozone changes coincide with high underlying albedos (either reflective surfaces, such

ACPD
12, 26047–26097, 2012

as deserts or ice, or low cloud). RFs are reduced over high altitude regions (e.g. Tibet, Rockies, Greenland) as there is less air mass, and hence less column ozone (see Fig. 2). Figure 5 shows the normalised total RF ($mW\,m^{-2}\,DU^{-1}$) for MASKZMT; Fig. S5 is equivalent for all 17 models. Normalised RFs are highest in the tropics, where the temperature difference between the surface and tropopause is largest, and peak in relatively cloud-free regions over NW Australia. Similar distributions for normalised RFs have been found previously (e.g. Gauss et al., 2003, their Fig. 7).

In order to estimate the uncertainty associated with these RFs, we tested how the following processes and choices influenced results: (i) choice of tropopause definition; (ii) choice of radiation scheme; (iii) stratospheric adjustment; and (iv) treatment of clouds.

Tropopause definitions are problematic (e.g. Prather et al., 2011). The Edwards-Slingo (hereafter E-S) scheme was run for all models using the two different tropopause definitions (MASKZMT and MASK150). MASK150 was also used to define the troposphere in some of the other ACCMIP papers (e.g. Young et al., 2012a), and has been widely used in earlier studies (e.g. Prather et al., 2001; Stevenson et al., 2006). Radiation calculations with the different tropopause differ due to changes in: (i) tropospheric column ozone; (ii) the altitude of where the net flux changes are output; and (iii) the altitude above which stratospheric temperatures are adjusted. The initial temperature profile remains unchanged. Global mean 1850s–2000s column ozone changes are larger by 0.1–1.1 DU (1–12 %), and net ozone RFs larger by 5–41 $mW\,m^{-2}$ (1–10 %), with MASK150 compared to MASKZMT (Table 3; the ranges quoted cover the full model spread).

We additionally calculated instantaneous (i.e. without stratospheric temperature adjustment) tropospheric ozone RFs with the E-S scheme, both leaving clouds as before, and also for clear skies (i.e. removing all clouds). We only use a single representation of cloud distributions (from the 64-level HadAM3 model) in the E-S calculations; cloud fields from individual models were not used. We found very similar results for the influence of stratospheric adjustment and clouds in the E-S scheme for all models; results are summarised in Table 4. Stratospheric temperature adjustment changes the SW, LW

ACPD
12, 26047–26097, 2012

and net RFs, respectively, by: 0 %, −24 ± 1 %, and −20 ± 1 % for MASKZMT; and 0 %, −26 ± 1 %, and −22 ± 1 % for MASK150. Inclusion of clouds affects RFs by: 20 ± 4 %, −16 ± 1 %, and −12 ± 1 % for MASKZMT; and 21 ± 5 %, −16 ± 1 %, and −12 ± 1 % for MASK150. Quoted uncertainties are standard deviations across all the models. Model B sits close to the mean values. The Oslo radiation scheme repeated these calculations for just model B, and found (results in the same format as above) that stratospheric adjustment changes RFs by: 0, −21, and −17 %; whilst clouds change RFs by: 35, −30, −22 %. Thus stratospheric adjustment has a slightly smaller effect in the Oslo scheme compared to E-S, whereas clouds have a stronger influence. The Oslo radiation scheme uses its own cloud fields; we have not compared these to the cloud fields used in the E-S calculations.

Comparing the clear-sky instantaneous results between the E-S and Oslo schemes for MASK150 (Table 5) indicates that the Oslo LW RFs are 6 % lower than E-S, but that the SW RFs are 13 % higher. Since these differences are in opposite directions, the difference between schemes for the net RF is smaller (Oslo is 4 % less than E-S).

Comparing stratospherically adjusted RFs between these two schemes (Table 5) (for MASK150) shows that the SW RF is 24 % higher in the Oslo scheme, but the LW RF is 18 % lower, and the net RF is 10 % lower. A similar result is found when comparing the E-S and NCAR schemes (Table 5): the NCAR scheme has 17 % higher values for SW RF, 16 % lower LW RF values, and net RFs that are 10 % lower. These comparisons between radiation schemes are used to infer levels of uncertainty associated with radiation calculations (see Sect. 4).

3.1.2 Attribution experiments

A subset of six models ran a series of attribution experiments, based on the 2000s simulations (Tables 1 and 6). Specific drivers of ozone change (anthropogenic emissions of NO_x, CO, NMVOCs, and CH_4 concentrations) were individually reduced to 1850s levels. In all these experiments, the driving meteorology was identical to the base 2000s case; thus differences between simulations isolate the influence of the

ACPD
12, 26047–26097, 2012

specific component that is changed. For the methane case, concentrations were reduced to 1850s levels (~ 791 ppbv), and are fixed at this level. In the other experiments, methane was fixed at present-day levels (~ 1751 ppbv), and emissions were reduced to their 1850s levels. Fixing methane concentrations has important consequences for how these experiments are interpreted, and this set-up differs from previous approaches, where methane emissions were changed, and methane concentrations were allowed to respond (Shindell et al., 2005, 2009).

Differences in ozone fields between attribution experiments and the year 2000s base case suggests that the largest component of the 1850s–2000s ozone change comes from NO_x emissions, the next largest from changes in methane, and relatively small contributions from changes in CO and NMVOC emissions (e.g. Figs. S6 and S7 show ozone changes and radiative forcings for model B). However, by imposing fixed methane concentrations, these runs are out of equilibrium for methane (and hence ozone). Making the assumption that the base 1850s and 2000s runs are in equilibrium for methane (with methane concentration $[CH_4]_{base}$ and lifetime τ_{base}), we take diagnosed methane lifetimes from the attribution experiments (τ_{att}) and calculate equilibrium methane concentrations ($[CH_4]_{eq}$) for each attribution experiment. We apply the method described in West et al. (2007) and Fiore et al. (2009), using the following equation:

$$[CH_4]_{eq}=[CH_4]_{base}(\tau_{att}/\tau_{base})^f \quad (1)$$

where f is the methane adjustment factor, which we take to be 1.35 (Prather et al., 2012). Methane lifetimes are for the whole atmosphere; we use diagnosed tropospheric lifetimes (with respect to OH), and adjust to include losses in the stratosphere (120 yr lifetime) and soils (160 yr lifetime) (Table 7). Differences between these equilibrium methane concentrations and the observed year 2000s value were used to calculate a methane radiative forcing associated with attribution experiments #2–5. Methane RFs were calculated using global mean methane concentrations and the simple formula given by Ramaswamy et al. (2001; their Table 6.2). This methane adjustment will also

ACPD
12, 26047–26097, 2012

generate a further ozone change and radiative forcing – these have been estimated by assuming a linear scaling of the ozone RF found in each model's methane experiment.

For example, for model B, the NO_x experiment (#3) yields a methane lifetime of 11.60 yr, compared to the base year 2000s experiment (#1) value of 8.70 yr (Table 7). The longer lifetime reflects lower levels of OH due to the removal of NO_x emissions. If this experiment had been carried out with methane free to adjust, Eq. (1) indicates that methane would have responded by increasing from 1751 ppbv to an equilibrium level of 2581 ppbv (Table 7), generating a radiative forcing of 276 mW m^{-2}. Thus the methane radiative forcing associated with NO_x emission increases from the 1850s up to the 2000s is −276 mW m^{-2}. The associated extra ozone forcing, found by scaling model B's ozone response to methane, is −132 mW m^{-2}. Adding this to the ozone forcing found directly from the NO_x attribution experiment (193 mW m^{-2}) yields a net ozone forcing of 61 mW m^{-2} for model B (Table 8).

We further extend our analysis to include the impacts of CH_4, CO and NMVOC emissions on CO_2 concentrations. All these emissions oxidise to form CO_2 and therefore generate an additional RF (Table 9 and Supplement). Other effects, such as impacts of methane on stratospheric H_2O, or impacts of changes in oxidants on secondary aerosol (Shindell et al., 2009), are not included in our analysis. We summarise the average results of all the models that ran the attribution experiments in Table 9.

Based on this analysis, the tropospheric ozone RF can be attributed to emissions increases as follows: 52 % (CH_4), 21 % (NO_x), 17 % (CO) and 10 % (NMVOC). The sum of the contributions to ozone RF diagnosed from the individual experiments is 364 mW m^{-2}, compared to a mean result for the 1850s–2000s experiments by the same models of 385 mW m^{-2}. However, the sum of the indirect effects on methane must sum to zero, but actually sum to −98 mW m^{-2}, dominated by the large negative contribution from NO_x. This indicates some deficiencies in our analysis as non-linear coupled effects are not captured by our simple approach.

The mean changes in methane lifetime in the attribution experiments (Table 7) are: −16 % (CH_4), +40 % (NO_x), −7 % (CO) and −3 % (NMVOC). The estimation of

ACPD
12, 26047–26097, 2012

equilibrium methane concentrations from Eq. (1) is only valid for small perturbations to the methane lifetime (West et al., 2007). As such, the method is probably reasonable for the CO and NMVOC experiments, and possibly for the CH_4 experiments, but is likely to produce poor results for the large perturbations from the NO_x experiments. If we make the crude assumption that all of the error is in the $[CH_4]_{eq}$ values from the NO_x experiments, and force the sum of the indirect effects on methane to be zero, then the mean indirect RF for methane from NO_x must be $-229\,mW\,m^{-2}$ rather than the value of $-327\,mW\,m^{-2}$ in Table 9. The inferred ozone RF associated with the methane change will also reduce proportionately, increasing the net ozone RF associated with NO_x emissions from 76 to $119\,mW\,m^{-2}$. Applying these crude corrections, we find the relative contributions to the ozone RF are now: 47 % (CH_4), 29 % (NO_x), 15 % (CO) and 9 % (NMVOC). We consider these proportions to be more accurate than those without any corrections applied.

3.1.3 Experiments that isolate the climate change component

Most models performed the core 1850s and 2000s experiments with driving climates appropriate for these decades (Table 1). In addition, 10 models carried out sensitivity experiments with 2000s emissions, but driven by 1850s climate. By comparing runs with the same emissions, but different climates, we can diagnose the impact of climate change on tropospheric ozone. Figure 6 shows the impact of climate change from 1850s to 2000s on AZM and tropospheric column ozone, for the 10 models.

Modelled tropospheric ozone shows a range of responses to climate change. The largest overall response is seen in models G and H (the two GISS versions), where climate change is the main driver of the SH decreases in ozone seen in these models (Fig. S3). In these GISS integrations, the stratosphere also changes, so it is unclear if it is stratospheric change or climate change that is driving the SH decreases. The other model with large decreases in SH ozone (M), also changes its stratosphere in its climate change experiments, however the climate change experiment does not produce

ACPD
12, 26047–26097, 2012

the large SH decrease seen in the standard 1850s–2000s experiment, so the origin of this signal in this model remains unclear. Some models show increases in tropical mid- to upper tropospheric ozone, with these increases centred over the continents (G, H, and to a lesser extent O, F and L). All these models (except F) show (small) increases in lightning NO_x emissions (Table 2); however, other models that also show increases in lightning do not show obvious increases in tropical ozone (A, M, N and P). Most of the models show decreases in ozone, particularly in the tropical lower troposphere, which would be expected due to increases in water vapour and hence ozone destruction (e.g. Johnson et al., 2001). Several models also show indications of increases in the stratospheric source of ozone, e.g. in the sub-tropical jet region (A, F, I, L, and P). Similar features have been seen in some future simulations under climate change scenarios (e.g. Zeng and Pyle, 2003; Kawase et al., 2011). On average, the net impact of climate change on ozone is a small decrease in tropospheric ozone. Many of these climate change induced changes in ozone can be seen more strongly in results from associated experiments that fixed emissions at 2000s levels but simulated climate of the 2030s and 2100s (see Fig. S8).

3.2 Other simulations

Several models ran time slice simulations covering several intervening decades between the 1850s and 2000s, and also for the four future Representative Concentration Pathway scenarios (RCP2.6, RCP 4.5, RCP6.0 and RCP8.5) (Table 1). Young et al. (2012a) provide details of the changes in surface and tropospheric ozone from these simulations. Here, we use spatially resolved annual mean changes in tropospheric column ozone, and convolve these together with individual model's normalised ozone RFs (Fig. 5/S5), to estimate the RF for each timeslice experiment relative to the 1850s (Fig. 7). A subset of these results (for the 1980s, 2000s, 2030s and 2100s) are also presented in Table 10. Seasonal variations in both column changes and normalised RFs are not accounted for, and this indirect method of calculating RFs also assumes that the normalised ozone RF for 1850s–2000s does not change with time;

ACPD
12, 26047–26097, 2012

i.e. that the shape of the change in ozone vertical profile is temporally invariant. We consider that these approximations introduce only small errors in the estimates of ozone RF presented in Fig. 7 and Table 10.

Table 10 also shows mean values for selected time periods, constructed in three different ways: (i) using all available models for a given time slice; (ii) just using the four models (F, G, K and N) that ran all of the timeslices in Table 10; and (iii) using a subset of ten models (A, B, F, G, K, L, M, N, O and P) that ran all the time slices except those for RCP4.5 and RCP6.0. Comparing the mean values calculated by these different methods shows that there is little influence on the overall results (the maximum deviation is 0.024 $W m^{-2}$, or ~ 10 %, for RCP6.0 in 2100) of the variable model coverage of different timeslices.

4 Discussion and conclusions

With the MASKZMT tropopause, we find a mean value for the tropospheric ozone radiative forcing (1850s–2000s) of 356 $mW m^{-2}$, with a standard deviation across 17 models of ±58 $mW m^{-2}$ (±16 %) (Table 10). The median model has a value of 367 $mW m^{-2}$, and the full range spans 211–429 $mW m^{-2}$. The model at the low end of this range (model M) is an isolated outlier – the next lowest value is 297 $mW m^{-2}$ (Table 10). Using an alternate tropopause (MASK150), we find slightly higher values: 377 ± 65 $mW m^{-2}$ (±17 %) (Table 3). Values from the two sets of calculations differ by 6 %; this suggests that tropopause definition introduces an uncertainty of at least ±3 %.

These values were calculated by the Edwards and Slingo (1996) (E-S) radiation scheme. We find that the E-S radiation scheme gives net, stratospherically adjusted ozone RFs that are 10 % higher than comparable schemes from Oslo and NCAR (Table 5). Taking the mean of our values for the two different tropopauses with the E-S scheme (367 $mW m^{-2}$), and adjusting for the Oslo and NCAR schemes producing slightly lower values (i.e. giving equal weight to each radiation scheme by multiplying

ACPD
12, 26047–26097, 2012

by a factor of $(1.0 + 0.9 + 0.9)/3 = 0.93$), our best estimate of tropospheric ozone RF is $342\,\mathrm{mW\,m^{-2}}$.

Based on a comparison of instantaneous clear sky SW ozone RFs between the E-S and Oslo schemes (Table 5), we estimate radiative transfer schemes introduce uncertainty of about ±6 %. Clouds influence ozone RFs to different degrees in the E-S and Oslo schemes, and add uncertainty of at least ±7 % (Table 4). The influence of stratospheric adjustment also varies between the two schemes, adding uncertainty of about ±3 %. Based on a these individual uncertainties, and assuming they are independent, we estimate the overall uncertainty associated with the radiation scheme of about ±10 %, based on the square root of the sum of the squares (RSS). Combining these uncertainties with the model range (±17 %) and difference due to tropopause definition (±3 %), we estimate an overall (RSS) uncertainty of ±20 % from these factors.

Further sources of uncertainty in the ozone RF stem from uncertainties in precursor emissions (natural and anthropogenic), as well as changes in climate and stratospheric ozone. Most models predict relatively small impacts on tropospheric ozone via climate change up to present-day (Fig. 6), but these impacts may increase in future (Fig. S8). Uncertainties associated with these factors, and emissions in particular, are probably similar or larger than the ±20 % estimated above. We therefore estimate an overall uncertainty of ±30 % on our central estimate (Skeie et al., 2011, estimate the same value for uncertainty). Given the magnitude of the uncertainty, we quote values to two significant figures, giving our best estimate and uncertainty of $340 \pm 100\,\mathrm{mW\,m^{-2}}$. It should be noted that this value is for 1850s to 2000s (which we take to be 1855 to 2005). Skeie et al. (2011) calculated tropospheric ozone increases between 1750 and 1850 of 1.0 DU (using model B), suggesting an extra $42\,\mathrm{mW\,m^{-2}}$ should be added to give the RF from 1750 to 2005. Similarly, they calculate an increase from 2005 to 2010 of 0.25 DU, which would add a further $11\,\mathrm{mW\,m^{-2}}$. Hence for 1750–2010 our best estimate of tropospheric ozone RF is $400 \pm 120\,\mathrm{mW\,m^{-2}}$.

While it is well understood that increases in CH_4, NO_x, CO and NMVOCs have driven up tropospheric ozone, only one model has previously explored the relative

ACPD
12, 26047–26097, 2012

contributions of these different precursors (Shindell et al., 2005, 2009). Applying six different models here, we estimate that CH_4, NO_x, CO and NMVOCs are, respectively responsible for 47 % (full model range: 29–53 %), 29 % (23–46 %), 15 % (13–17 %) and 9 % (6–12 %) of the 1850s–2000s ozone RF. As can be seen from the model range, there remains some uncertainty over the exact values for these fractions; an important source of uncertainty stems from extrapolating results from the experiments to yield equilibrium methane concentrations. Model P is an outlier, the only model that finds NO_x emissions to be a larger driver of tropospheric ozone RF than CH_4 emissions. These contributions compare to values of 51 % (CH_4), 15 % (NO_x), and 33 % (CO and NMVOC combined) from Shindell et al. (2005), as reported in IPCC-AR4 (Forster et al., 2007, Table 2.13). The results from Shindell et al. (2009) indicate a split of: 74 % (CH_4), 11 % (NO_x), 13 % (CO) and 2 % (NMVOCs), which is outside the model range (except for CO) found in this study. The reasons for differences between the two Shindell et al. studies and the results presented here are unclear, but do point to significant model diversity and uncertainty in the drivers of tropospheric ozone increases. Using the fractions from this study, we find that for 1750–2010, the tropospheric ozone RF of 400 mW m^{-2} can be apportioned to increased emissions as follows: 188 mW m^{-2} from CH_4, 116 mW m^{-2} from NO_x, 60 mW m^{-2} from CO and 36 mW m^{-2} from NMVOC. By affecting methane's lifetime, these emissions have also influenced the methane RF, and we find values of: +147, −229, +59 and +23 mW m^{-2} for CH_4, NO_x, CO and NMVOC, respectively. With the exception of NO_x, all these emissions oxidise to form CO_2 and therefore generate an additional RF (Table 9 and Supplement). There are further RF impacts of these emissions via secondary aerosol formation and changes in stratospheric water vapour that have not been estimated here (see Shindell et al., 2009). Based on their impacts on CO_2, CH_4 and tropospheric ozone, we estimate overall emissions based RFs for CH_4, NO_x, CO and NMVOC of: +780, −110, +210 and +90 mW m^{-2}, respectively.

Normalising the tropospheric ozone RF by the change in tropospheric column ozone (Fig. 5), we find a global mean value of 42 mW m^{-2} DU^{-1} (using MASKZMT). This is

ACPD
12, 26047–26097, 2012

similar to values from earlier studies, namely 42 mW m^{-2} DU^{-1} (Ramaswamy et al., 2001; their Table 6.3 – a mean value from 11 studies) and 36 mW m^{-2} DU^{-1} (Gauss et al., 2003; their Table 3 – a mean value from 11 models simulating 2000 to 2100 changes). Normalised forcings vary slightly between models (Fig. S5), reflecting differing ozone changes at different latitudes and heights (Fig. S3).

Using the normalised forcing from each model, together with the simulated tropospheric column ozone change, we have calculated RFs for each model for each available timeslice (Fig. 7). Although different subsets of models ran the timeslices, we find this has only a small influence on calculated multi-model mean values (Table 10). Making the harmonisation to our best estimate of 1850s–2000s RF, we estimate tropospheric ozone RFs (relative to the 1850s) of 80, 290 and 340 mW m^{-2} for the 1930s, 1980s and 2000s, respectively. For the RCP2.6 scenario, we find values of 310 and 160 mW m^{-2} for the 2030s and 2100s; for RCP4.5: 380 and 260 mW m^{-2}; for RCP6.0: 330 and 240 mW m^{-2}; and for RCP8.5: 420 and 560 mW m^{-2} (again, all relative to the 1850s). All these have similar uncertainties to our pre-industrial to present-day estimate, which is at least ±30 %. Uncertainties are arguably smaller for the future scenarios, as they are for exactly prescribed emissions; however, other sources of uncertainty increase, in particular the effects of climate change, land-use change and changing stratospheric ozone on tropospheric ozone.

Over the 1850s–2000s, climate change has had relatively small influences on tropospheric ozone in most models (Fig. 6), but is more important in some (e.g. models G and H). In the future, models suggest these changes will generally increase, with models displaying some coherent responses (Fig. S8). All models suggest ozone in the tropical lower troposphere will reduce, mainly due to warmer temperatures and higher water vapour concentrations. Most models indicate that ozone will increase in the subtropical to mid-latitude upper troposphere, due to a combination of increased lightning NO_x production (Schumann and Huntrieser, 2007), and an increase of stratosphere-to-troposphere transport (Hegglin and Shepherd, 2009), as suggested by some earlier studies.

ACPD
12, 26047–26097, 2012

This study provides an up-to-date assessment of the tropospheric ozone radiative forcing included in the current generation of Earth System Models participating in CMIP5. Although the magnitudes and uncertainties in the tropospheric ozone radiative forcing are rather similar to previous assessments, this study sets a useful benchmark for future work. There remains significant diversity in model response to ozone precursor emissions, and this range of model behaviour needs to be better understood if models are to provide useful advice to policymakers. Future studies should target the key processes that control tropospheric ozone and its precursors.

Supplementary material related to this article is available online at: http://www.atmos-chem-phys-discuss.net/12/26047/2012/acpd-12-26047-2012-supplement.pdf.

Acknowledgements. ACCMIP is organized under the auspices of Atmospheric Chemistry and Climate (AC&C), a project of International Global Atmospheric Chemistry (IGAC) and Stratospheric Processes And their Role in Climate (SPARC) under the International Geosphere-Biosphere Project (IGBP) and World Climate Research Program (WCRP). The authors are grateful to the British Atmospheric Data Centre (BADC), which is part of the NERC National Centre for Atmospheric Science (NCAS), for collecting and archiving the ACCMIP data. DS thanks James Manners for assistance in setting up the E-S radiation code. GAF, STR and WJC were supported by the Joint DECC and Defra Integrated Climate Programme (GA01101) and the Defra SSNIP air quality contract AQ 0902. GZ acknowledges NIWA HPCF facility and funding from New Zealand Ministry of Science and Innovation. The CESM project is supported by the National Science Foundation and the Office of Science (BER) of the US Department of Energy. The National Center for Atmospheric Research is operated by the University Corporation for Atmospheric Research under sponsorship of the National Science Foundation. The work of DB and PC was funded by the US Dept. of Energy (BER), performed under the auspices of LLNL under Contract DE-AC52-07NA27344, and used the supercomputing resources of NERSC under contract No. DE-AC02-05CH11231. VN and LWH acknowledge efforts of GFDL's Global Atmospheric Model Development Team in the development of the GFDL-AM3

ACPD
12, 26047–26097, 2012

and Modeling Services Group for assistance with data processing. The GEOSCCM work was supported by the NASA Modeling, Analysis and Prediction program, with computing resources provided by NASA's High-End Computing Program through the NASA Advanced Supercomputing Division. The MIROC-CHEM calculations were perfomed on the NIES supercomputer system (NEC SX-8R), and supported by the Environment Research and Technology Development Fund (S-7) of the Ministry of the Environment, Japan. The STOC-HadAM3 work was supported by cross council grant NE/I008063/1, and used facilities provided by the UK's national high-performance computing service, HECToR, through Computational Modelling Services (CMS), part of the NERC National Centre for Atmospheric Science (NCAS). The LMDz-OR-INCA simulations were done using computing ressources provided by the CCRT/GENCI computer center of the CEA. The CICERO-OsloCTM2 simulations were done within the projects SLAC (Short Lived Atmospheric Components) and EarthClim funded by the Norwegian Research Council. The MOCAGE simulations were supported by Météo-France and CNRS. Supercomputing time was provided by Météo-France/DSI supercomputing center. DTS and YHL acknowledge support from the NASA MAP and ACMAP programs. DP would like to thank the Canadian Foundation for Climate and Atmospheric Sciences for their long-running support of CMAM development. AC was supported by the SciDAC program of the Dept. of Energy.

References

Andersson, C. and Engardt, M.: European ozone in a future climate: importance of changes in dry deposition and isoprene emissions, J. Geophys. Res.-Atmos., 115, D02303, doi:10.1029/2008JD011690, 2010.

Arneth, A., Sitch, S., Bondeau, A., Butterbach-Bahl, K., Foster, P., Gedney, N., de Noblet-Ducoudré, N., Prentice, I. C., Sanderson, M., Thonicke, K., Wania, R., and Zaehle, S.: From biota to chemistry and climate: towards a comprehensive description of trace gas exchange between the biosphere and atmosphere, Biogeosciences, 7, 121–149, doi:10.5194/bg-7-121-2010, 2010.

Berntsen, T. K., Isaksen, I. S. A., Myhre, G., Fuglestvedt, J., Stordal, F., Larsen, T., Freckleton, R., and Shine, K. P.: Effects of anthropogenic emissions on tropospheric ozone and its radiative forcing, J. Geophys. Res., 102, 28101–28126, 1997.

ACPD

12, 26047–26097, 2012

Bowman, K., Shindell, D., Worden, H., Lamarque, J. F., Young, P. J., Stevenson, D., Qu, Z., de la Torre, M., Bergmann, D., Cameron-Smith, P., Collins, W. J., Doherty, R., Dalsøren, S., Faluvegi, G., Folberth, G., Horowitz, L. W., Josse, B., Lee, Y. H., MacKenzie, I., Myhre, G., Nagashima, T., Naik, V., Plummer, D., Rumbold, S., Skeie, R., Strode, S., Sudo, K., Szopa, S., Voulgarakis, A., Zeng, G., Kulawik, S., and Worden, J.: Observational constraints on ozone radiative forcing from the Atmospheric Chemistry Climate Model Intercomparison Project (ACCMIP), Atmos. Chem. Phys. Discuss., 12, 23603–23644, doi:10.5194/acpd-12-23603-2012, 2012.

Cionni, I., Eyring, V., Lamarque, J. F., Randel, W. J., Stevenson, D. S., Wu, F., Bodeker, G. E., Shepherd, T. G., Shindell, D. T., and Waugh, D. W.: Ozone database in support of CMIP5 simulations: results and corresponding radiative forcing, Atmos. Chem. Phys., 11, 11267–11292, doi:10.5194/acp-11-11267-2011, 2011.

Crutzen, P. J.: Photochemical reactions initiated by and influencing ozone in the unpolluted troposphere, Tellus, 26, 47–57, 1974.

Crutzen, P. J. and Zimmerman, P. H.: The changing photochemistry of the troposphere, Tellus, 43, 136–151, 1991.

Derwent, R. G., Jenkin, M. E., and Saunders, S. M.: Photochemical ozone creation potentials for a large number of reactive hydrocarbons under European conditions, a large number of reactive hydrocarbons under European conditions, Atmos. Environ., 30, 181–199, doi:10.1016/1352-2310(95)00303-G, 1996.

Edwards, J. M. and Slingo, A.: Studies with a flexible new radiation code. I: Choosing a configuration for a large-scale model, Q. J. Roy. Meteorol. Soc., 122, 689–719, 1996.

Engel, A., Möbius, T., Bönisch, H., Schmidt, U., Heinz, R., Levin, I., Atlas, E., Aoki, S., Nakazawa, T., Sugawara, S., Moore, F., Hurst, D., Elkins, J., Schauffler, S., Andrews, A., and Boering, K.: Age of stratospheric air unchanged within uncertainties over the past 30 years, Nat. Geosci., 2, 28–31, doi:10.1038/ngeo388, 2009.

Fiore, A. M., Dentener, F. J., Wild, O., Cuvelier, C., Schultz, M. G., Hess, P., Textor, C., Schulz, M., Doherty, R. M., Horowitz, L. W., MacKenzie, I. A., Sanderson, M. G., Shindell, D. T., Stevenson, D. S., Szopa, S., Van Dingenen, R., Zeng, G., Atherton, C., Bergmann, D., Bey, I., Carmichael, G., Collins, W. J., Duncan, B. N., Faluvegi, G., Folberth, G., Gauss, M., Gong, S., Hauglustaine, D., Holloway, T., Isaksen, I. S. A., Jacob, D. J., Jonson, J. E., Kaminski, J. W., Keating, T. J., Lupu, A., Marmer, E., Montanaro, V., Park, R. J., Pitari, G., Pringle, K. J., Pyle, J. A., Schroeder, S., Vivanco, M. G., Wind, P., Wojcik, G., Wu, S., and Zuber, A.:

ACPD
12, 26047–26097, 2012

Multi-model estimates of intercontinental source-receptor relationships for ozone pollution, J. Geophys. Res., 114, D04301, doi:10.1029/2008JD010816, 2009.

Fishman, J., Watson, C. E., Larsen, J. C., and Logan, J. A.: Distribution of tropospheric ozone determined from satellite data, J. Geophys. Res., 95, 3599–3617, 1990.

Forster, P., Ramaswamy, V., Artaxo, P., Berntsen, T., Betts, R., Fahey, D. W., Haywood, J. L., Lowe, D. C., Myhre, G., Nganga, J., Prinn, R., Raga, G., Schulz, M., and Van Dorland, R.: Changes in atmospheric constituents and in radiative forcing, in: Climate Change 2007: The Physical Science Basis, edited by: Solomon, S., Cambridge University Press, New York, 2007.

Fowler, D., Pilegaard, K., Sutton, M. A., Ambus, P., Raivonen, M., Duyzer, J., Simpson, D., Fagerli, H., Fuzzi, S., Schjoerring, J. K., Granier, C., Neftel, A., Isaksen, I. S. A., Laj, P., Maione, M., Monks, P. S., Burkhardt, J., Daemmgen, U., Neirynck, J., Personne, E., Wichink-Kruit, R., Butterbach-Bahl, K., Flechard, C., Tuovinen, J. P., Coyle, M., Gerosa, G., Loubet, B., Altimir, N., Gruenhage, L., Ammann, C., Cieslik, S., Paoletti, E., Mikkelsen, T. N., Ro-Poulsen, H., Cellier, P., Cape, J. N., Horváth, L., Loreto, F., Niinemets, Ü., Palmer, P. I., Rinne, J., Misztal, P., Nemitz, E., Nilsson, D., Pryor, S., Gallagher, M. W., Vesala, T., Skiba, U., Brüggemann, N., Zechmeister-Boltenstern, S., Williams, J., O'Dowd, C., Facchini, M. C., de Leeuw, G., Flossman, A., Chaumerliac, N., and Erisman, J. W.: Atmospheric composition change: ecosystems–atmosphere interactions, Atmos. Environ., 43, 5193–5267, 2009.

Ganzeveld, L., Bouwman, L., Stehfest, E., Vuuren, D. P. V., Eickhout, B., and Lelieveld, J.: Impact of future land use and land cover changes on atmospheric chemistry-climate interactions, J. Geophys. Res., 115, D23301, doi:10.1029/2010JD014041, 2010.

Gauss, M., Myhre, G., Pitari, G., Prather, M. J., Isaksen, I. S. A., Berntsen, T. K., Brasseur, G. P., Dentener, F. J., Derwent, R. G., Hauglustaine, D. A., Horowitz, L. W., Jacob, D. J., Johnson, M., Law, K. S., Mickley, L. J., Muller, J.-F., Plantevin, P.-H., Pyle, J. A., Rogers, H. L., Stevenson, D. S., Sundet, J. K., van Weele, M., and Wild, O.: Radiative forcing in the 21st century due to ozone changes in the troposphere and the lower stratosphere, J. Geophys. Res., 108, D94292, doi:10.1029/2002JD002624, 2003.

Gauss, M., Myhre, G., Isaksen, I. S. A., Grewe, V., Pitari, G., Wild, O., Collins, W. J., Dentener, F. J., Ellingsen, K., Gohar, L. K., Hauglustaine, D. A., Iachetti, D., Lamarque, F., Mancini, E., Mickley, L. J., Prather, M. J., Pyle, J. A., Sanderson, M. G., Shine, K. P., Stevenson, D. S., Sudo, K., Szopa, S., and Zeng, G.: Radiative forcing since preindustrial times

ACPD
12, 26047–26097, 2012

due to ozone change in the troposphere and the lower stratosphere, Atmos. Chem. Phys., 6, 575–599, doi:10.5194/acp-6-575-2006, 2006.
Hansen, J., Sato, M., and Ruedy, R.: Radiative forcing and climate response, J. Geophys. Res., 102, 6831–6864, 1997.
Hegglin, M. I. and Shepherd, T. G.: Large climate-induced changes in ultraviolet index and stratosphere-to-troposphere ozone flux, Nat. Geosci., 2, 687–691, doi:10.1038/ngeo604, 2009.
Hough, A. E. and Derwent, R. G.: Changes in the global concentration of tropospheric ozone due to human activities, Nature, 344, 645–648; doi:10.1038/344645a0, 1990.
Hsu, J. and Prather, M. J.:, Stratospheric variability and tropospheric ozone, J. Geophys. Res., 114, D06102, doi:10.1029/2008JD010942, 2009.
Huijnen, V., Williams, J., van Weele, M., van Noije, T., Krol, M., Dentener, F., Segers, A., Houweling, S., Peters, W., de Laat, J., Boersma, F., Bergamaschi, P., van Velthoven, P., Le Sager, P., Eskes, H., Alkemade, F., Scheele, R., Nédélec, P., and Pätz, H.-W.: The global chemistry transport model TM5: description and evaluation of the tropospheric chemistry version 3.0, Geosci. Model Dev., 3, 445–473, doi:10.5194/gmd-3-445-2010, 2010.
Isaksen, I. S. A., Granier, C., Myhre, G., Berntsen, T. K., Dalsøren, S. B., Gauss, M., Klimont, Z., Benestad, R., Bousquet, P., Collins, W., Cox, T., Eyring, V., Fowler, D., Fuzzi, S., Jockel, P., Laj, P., Lohmann, U., Maione, M., Monks, P., Prevot, A. S. H., Raes, F., Richter, A., Rognerud, B., Schulz, M., Shindell, D., Stevenson, D. S., Storelvmo, T., Wang, W.-C., van Weele, M., Wild, M., and Wuebbles, D.: Atmospheric composition change: climate-chemistry interactions, Atmos. Environ., 43, 5138–5192, doi:10.1016/j.atmosenv.2009.08.003, 2009.
Johnson, C. E., Stevenson, D. S., Collins, W. J., and Derwent, R. G.: Role of climate feedback on methane and ozone studied with a coupled ocean–atmosphere-chemistry model, Geophys. Res. Lett., 28, 1723–1726, 2001.
Kawase, H., Nagashima, T., Sudo, K., and Nozawa, T.: Future changes in tropospheric ozone under representative concentration pathways (RCPs), Geophys. Res. Lett., 38, L05801, doi:10.1029/2010GL046402, 2011.
Lacis, A. A., Wuebbles, D. J., and Logan, J. A.: Radiative forcing of climate by changes in the vertical distribution of ozone, J. Geophys. Res., 95, 9971–9981, 1990.
Lamarque, J.-F., Bond, T. C., Eyring, V., Granier, C., Heil, A., Klimont, Z., Lee, D., Liousse, C., Mieville, A., Owen, B., Schultz, M. G., Shindell, D., Smith, S. J., Stehfest, E., Van Aardenne, J., Cooper, O. R., Kainuma, M., Mahowald, N., McConnell, J. R., Naik, V., Riahi, K.,

ACPD
12, 26047–26097, 2012

and van Vuuren, D. P.: Historical (1850–2000) gridded anthropogenic and biomass burning emissions of reactive gases and aerosols: methodology and application, Atmos. Chem. Phys., 10, 7017–7039, doi:10.5194/acp-10-7017-2010, 2010.

Lamarque, J.-F., Shindell, D. T., Josse, B., Young, P. J., Cionni, I., Eyring, V., Bergmann, D., Cameron-Smith, P., Collins, W. J., Doherty, R., Dalsoren, S., Faluvegi, G., Folberth, G., Ghan, S. J., Horowitz, L. W., Lee, Y. H., MacKenzie, I. A., Nagashima, T., Naik, V., Plummer, D., Righi, M., Rumbold, S., Schulz, M., Skeie, R. B., Stevenson, D. S., S. Strode, Sudo, K., Szopa, S., Voulgarakis, A., and Zeng, G.: The Atmospheric Chemistry and Climate Model Intercomparison Project (ACCMIP): overview and description of models, simulations and climate diagnostics, Geosci. Model Dev., in review, 2012.

Lee, Y. H., Lamarque, J.-F., Flanner, M. G., Jiao, C., Shindell, D. T., Berntsen, T., Bisiaux, M. M., Cao, J., Collins, W. J., Curran, M., Edwards, R., Faluvegi, G., Ghan, S., Horowitz, L. W., McConnell, J. R., Myhre, G., Nagashima, T., Naik, V., Rumbold, S. T., Skeie, R. B., Sudo, K., Takemura, T., and Thevenon, F.: Evaluation of preindustrial to present-day black carbon and its albedo forcing from ACCMIP (Atmospheric Chemistry and Climate Model Intercomparison Project), Atmos. Chem. Phys. Discuss., 12, 21713–21778, doi:10.5194/acpd-12-21713-2012, 2012.

Li, D. and Shine, K. P.: A 4-D ozone climatology for UGAMP models, UGAMP internal report, University of Reading, http://badc.nerc.ac.uk/data/ugamp-o3-climatology (last access: October 2012), 1995.

Lin, P., Fu, Q., Solomon, S., and Wallace, J. M.: Temperature trend patterns in Southern Hemisphere high latitudes: novel indicators of stratospheric change, J. Climate, 22, 6325–6340, doi:10.1175/2009JCLI2971.1, 2009.

Logan, J. A.: An analysis of ozonesonde data for the troposphere: recommendations for testing 3-D models, and development of a gridded climatology for tropospheric ozone, J. Geophys. Res., 104, 16115–16149, 1999.

McLinden, C. A., Olsen, S. C., Hannegan, B., Wild, O., Prather, M. J., and Sundet, J.: Stratospheric ozone in 3-D models: a simple chemistry and the cross-tropopause flux, J. Geophys. Res., 105, 14653–14666, 2000.

Meinshausen, M., Smith, S. J., Calvin, K., Daniel, J. S., Kainuma, M. L. T., Lamarque, J.-F., Matsumoto, K., Montzka, S. A., Raper, S. C. B., Riahi, K., Thomson, A., Velders, G. J. M., and van Vuuren, D. P. P.: The RCP greenhouse gas concentrations and their extensions from 1765 to 2300, Climatic Change, 109, 213–241, doi:10.1007/s10584-011-0156-z, 2011.

ACPD
12, 26047–26097, 2012

Myhre, G. and Stordal, F.: Role of spatial and temporal variations in the computation of radiative forcing and GWP, J. Geophys. Res.-Atmos., 102, 11181–11200, 1997.

Myhre, G., Shine, K. P., Radel, G., Gauss, M., Isaksen, I. S. A., Tang, Q., Prather, M. J., Williams, J. E., van Velthoven, P., Dessens, O., Koffi, B., Szopa, S., Hoor, P., Grewe, V., Borken-Kleefeld, J., Berntsen, T. K., and Fuglestvedt, J. S.: Radiative forcing due to changes in ozone and methane caused by the transport sector, Atmos. Environ., 45, 387–394, 2011.

Oltmans, S. J., Lefohn, A. S., Harris, J. M., Galbally, I., Scheel, H. E., Bodeker, G., Brunke, E., Claude, H., Tarasick, D., Johnson, B. J., Simmonds, P., Shadwick, D., Anlauf, K., Hayden, K., Schmidlin, F., Fujimoto, T., Akagi, K., Meyer, C., Nichol, S., Davies, J., Redondas, A., and Cuevas, E.: Long-term changes in tropospheric ozone, Atmos. Environ., 40, 3156–3173, 2006.

Pavelin, E. G., Johnson, C. E., Rughooputh, S., and Toumi, R.: Evaluation of pre-industrial surface ozone measurements made using Schönbein's method, Atmos. Environ., 33, 919–929, doi:10.1016/S1352-2310(98)00257-X, 1999.

Pope, V. D., Gallani, M. L., Rowntree, P. R., and Stratton, R. A.: The impact of new physical parameterizations in the Hadley Centre climate model: HadAM3, Clim. Dynam., 16, 123–146, doi:10.1007/s003820050009, 2000.

Prather, M. J., Ehhalt, D., Dentener, F., Derwent, R., Dlugokencky, E., Holland, E., Isaksen, I., Katima, J., Kirchoff, V., Matson, P., Midgley, P., and Wang, M.: Atmospheric chemistry and greenhouse gases, in: Climate Change 2001: The Scientific Basis, Contribution of Working Group I to the Third Assessment Report of the Intergovernmental Panel on Climate Change, edited by: Houghton, J. T., Ding, Y., Griggs, D. J., Noguer, M., van der Linden, P. J., Dai, X., Maskell, K., and Johnson, C. A., Cambridge University Press, Cambridge, UK, 329–287, 2001.

Prather, M. J., Zhu, X., Tang, Q., Hsu, J., and Neu, J. L.: An atmospheric chemist in search of the tropopause, J. Geophys. Res., 116, D04306, doi:10.1029/2010JD014939, 2011.

Prather, M. J., Holmes, C. D., and Hsu, J.: Reactive greenhouse gas scenarios: systematic exploration of uncertainties and the role of atmospheric chemistry, Geophys. Res. Lett., 39, L09803, doi:10.1029/2012GL051440, 2012.

Prinn, R. G., Weiss, R. F., Fraser, P. J., Simmonds, P. G., Cunnold, D. M., Alyea, F. N., O'Doherty, S., Salameh, P., Miller, B. R., Huang, J., Wang, R. H. J., Hartley, D. E., Harth, C., Steele, L. P., Sturrock, G., Midgley, P. M., and McCulloch, A.: A history of chemically and

ACPD
12, 26047–26097, 2012

radiatively important gases in air deduced from ALE/GAGE/AGAGE, J. Geophys. Res., 105, 17751–17792, 2000.
Ramanathan, V. and Dickinson, R. E.: Role of stratospheric ozone in the zonal and seasonal radiative energy balance of the Earth-troposphere system, J. Atmos. Sci., 36, 1084–1104, 1979.
Ramaswamy, V., Boucher, O., Haigh, J., Hauglustaine, D., Haywood, J., Myhre, G., Nakajima, T., Shi, G. Y., and Solomon, S.: Radiative forcing of climate change, in: Climate Change 2001: The Scientific Basis, Contribution of Working Group I to the Third Assessment Report of the Intergovernmental Panel on Climate Change, edited by: Houghton, J. T., Ding, Y., Griggs, D. J., Noguer, M., van der Linden, P. J., Dai, X., Maskell, K., and Johnson, C. A., Cambridge Univ. Press, New York, 349–416, 2001.
Ray, E. A., Moore, F. L., Rosenlof, K. H., Davis, S. M., Boenisch, H., Morgenstern, O., Smale, D., Rozanov, E., Hegglin, M., Pitari, G., Mancini, E., Braesicke, P., Butchart, N., Hardiman, S., Li, F., Shibata, K., and Plummer, D. A.: Evidence for changes in stratospheric transport and mixing over the past three decades based on multiple data sets and tropical leaky pipe analysis, J. Geophys. Res., 115, D21304, doi:10.1029/2010JD014206, 2010.
Rubin, M. B.: The history of ozone, the Schönbein period, 1839–1868, Bull. Hist. Chem., 26, 40–56, 2001.
Sanderson, M. G., Collins, W. J., Hemming, D. L., and Betts, R. A.: Stomatal conductance changes due to increasing carbon dioxide levels: projected impact on surface ozone levels, Tellus B, 59, 404, doi:10.1111/j.1600-0889.2007.00277.x, 2007.
Sayer, A. M., Poulsen, C. A., Arnold, C., Campmany, E., Dean, S., Ewen, G. B. L., Grainger, R. G., Lawrence, B. N., Siddans, R., Thomas, G. E., and Watts, P. D.: Global retrieval of ATSR cloud parameters and evaluation (GRAPE): dataset assessment, Atmos. Chem. Phys., 11, 3913–3936, doi:10.5194/acp-11-3913-2011, 2011.
Schumann, U. and Huntrieser, H.: The global lightning-induced nitrogen oxides source, Atmos. Chem. Phys., 7, 3823–3907, doi:10.5194/acp-7-3823-2007, 2007.
Shindell, D. T., Faluvegi, G., Bell, N., and Schmidt, G.: An emissions-based view of climate forcing by methane and tropospheric ozone, Geophys. Res. Lett., 32, L04803, doi:10.1029/2004GL021900, 2005.
Shindell, D. T., Faluvegi, G., Koch, D. M., Schmidt, G. A., Unger, N., and Bauer, S. E.: Improved attribution of climate forcing to emissions, Science, 326, 716–718, doi:10.1126/science.1174760, 2009.

ACPD
12, 26047–26097, 2012

Shindell, D. T., Lamarque, J.-F., Schulz, M., Flanner, M., Jiao, C., Chin, M., Young, P., Lee, Y. H., Rotstayn, L., Milly, G., Faluvegi, G., Balkanski, Y., Collins, W. J., Conley, A. J., Dalsoren, S. B., Easter, R., Ghan, S., Horowitz, L., Liu, X., Myhre, G., Nagashima, T., Naik, V., Rumbold, S., Skeie, R., Sudo, K., Szopa, S., Takemura, T., Voulgarakis, A., and Yoon, J.-H.: Radiative forcing in the ACCMIP historical and future climate simulations, Atmos. Chem. Phys., in review, 2012.

Skeie, R. B., Berntsen, T. K., Myhre, G., Tanaka, K., Kvalevåg, M. M., and Hoyle, C. R.: Anthropogenic radiative forcing time series from pre-industrial times until 2010, Atmos. Chem. Phys., 11, 11827–11857, doi:10.5194/acp-11-11827-2011, 2011.

Sitch, S., Cox, P. M., Collins, W. J., and Huntingford, C.: Indirect radiative forcing of climate change through ozone effects on the land-carbon sink, Nature, 448, 791–795, doi:10.1038/nature06059, 2007.

SPARC-CCMVal: SPARC Report on the Evaluation of Chemistry-Climate Models, edited by: Eyring, V., Shepherd, T. G., and Waugh, D. W., SPARC Report No. 5, WCRP-132, WMO/TD-No. 1526, Geneva, available at: http://www.atmosp.physics.utoronto.ca/SPARC (last access: October 2012), 2010.

Staehelin, J., Thudium, J., Buehler, R., Volz-Thomas, A., and Graber, W.: Trends in surface ozone concentrations at Arosa (Switzerland), Atmos. Environ., 28, 75–87, 1994.

Stamnes, K., Tsay, S. C., Wiscombe, W., and Jayaweera, K.: Numerically stable algorithm for discrete-ordinate-method radiative-transfer in multiple-scattering and emitting layered media, Appl. Optics, 27, 2502–2509, 1988.

Stevenson, D. S., Dentener, F. J., Schultz, M. G., Ellingsen, K., van Noije, T. P. C., Wild, O., Zeng, G., Amann, M., Atherton, C. S., Bell, N., Bergmann, D. J., Bey, I., Butler, T., Cofala, J., Collins, W. J., Derwent, R. G., Doherty, R. M., Drevet, J., Eskes, H. J., Fiore, A. M., Gauss, M., Hauglustaine, D. A., Horowitz, L. W., Isaksen, I. S. A., Krol, M. C., Lamarque, J.-F., Lawrence, M. G., Montanaro, V., Muller, J.-F., Pitari, G., Prather, M. J., Pyle, J. A., Rast, S., Rodriguez, J. M., Sanderson, M. G., Savage, N. H., Shindell, D. T., Strahan, S. E., Sudo, K., and Szopa, S.: Multimodel ensemble simulations of present-day and near-future tropospheric ozone, J. Geophys. Res., 111, D08301, doi:10.1029/2005JD006338, 2006.

Stohl, A., Bonasoni, P., Cristofanelli, P., Collins, W., Feichter, J., Frank, A., Forster, C., Gerasopoulos, E., Gaggeler, H., James, P., Kentarchos, T., Kromp-Kolb, H., Kruger, B., Land, C., Meloen, J., Papayannis, A., Priller, A., Seibert, P., Sprenger, M., Roelofs, G. J., Scheel, H. E., Schnabel, C., Siegmund, P., Tobler, L., Trickl, T., Wernli, H., Wirth, V., Zanis, P., and

ACPD
12, 26047–26097, 2012

Zerefos, C.: Stratosphere–troposphere exchange: a review, and what we have learned from STACCATO, J. Geophys. Res., 108, 8516, doi:10.1029/2002JD002490, 2003.
Thouret, V., Cammas, J.-P., Sauvage, B., Athier, G., Zbinden, R., Nédélec, P., Simon, P., and Karcher, F.: Tropopause referenced ozone climatology and inter-annual variability (1994–2003) from the MOZAIC programme, Atmos. Chem. Phys., 6, 1033–1051, doi:10.5194/acp-6-1033-2006, 2006.
Tian, W. and Chipperfield, M. P.: A new coupled chemistry-climate model for the stratosphere: the importance of coupling for future O_3-climate predictions, Q. J. Roy. Meteorol. Soc., 131, 281–303, doi:10.1256/qj.04.05, 2005.
Volz, A. and Kley, D.: Evaluation of the Montsouris series of ozone measurements made in the nineteenth century, Nature, 332, 240–242, doi:10.1038/332240a0, 1988.
Von Hardenberg, J., Vozella, L., Tomasi, C., Vitale, V., Lupi, A., Mazzola, M., van Noije, T. P. C., Strunk, A., and Provenzale, A.: Aerosol optical depth over the Arctic: a comparison of ECHAM-HAM and TM5 with ground-based, satellite and reanalysis data, Atmos. Chem. Phys., in press, 2012.
Voulgarakis, A. et al.: Simulations of present-day and future OH and methane lifetime in the ACCMIP project, Atmos. Chem. Phys., in press, 2012.
Walters, D. N., Best, M. J., Bushell, A. C., Copsey, D., Edwards, J. M., Falloon, P. D., Harris, C. M., Lock, A. P., Manners, J. C., Morcrette, C. J., Roberts, M. J., Stratton, R. A., Webster, S., Wilkinson, J. M., Willett, M. R., Boutle, I. A., Earnshaw, P. D., Hill, P. G., MacLachlan, C., Martin, G. M., Moufouma-Okia, W., Palmer, M. D., Petch, J. C., Rooney, G. G., Scaife, A. A., and Williams, K. D.: The Met Office Unified Model Global Atmosphere 3.0/3.1 and JULES Global Land 3.0/3.1 configurations, Geosci. Model Dev., 4, 919–941, doi:10.5194/gmd-4-919-2011, 2011.
Wang, Y. and Jacob, D. J.: Anthropogenic forcing on tropospheric ozone and OH since preindustrial times, J. Geophys. Res., 103, 31123–31135, 1998.
West, J. J., Fiore, A. M., Naik, V., Horowitz, L. W., Schwarzkopf, M. D., and Mauzerall, D. L.: Ozone air quality and radiative forcing consequences of changes in ozone precursor emissions, Geophys. Res. Lett., 34, L06806, doi:10.1029/2006GL029173, 2007.
Wolff, E. W.: Greenhouse gases in the Earth system: a palaeoclimate perspective, Philos. T. Roy. Soc. Lond., 369, 2133–2147, 2011.

ACPD
12, 26047–26097, 2012

Wu, S., Mickley, L. J., Kaplan, J. O., and Jacob, D. J.: Impacts of changes in land use and land cover on atmospheric chemistry and air quality over the 21st century, Atmos. Chem. Phys., 12, 1597–1609, doi:10.5194/acp-12-1597-2012, 2012.

Young, P. J., Archibald, A. T., Bowman, K. W., Lamarque, J.-F., Naik, V., Stevenson, D. S., Tilmes, S., Vougarakis, A., Wild, O., Bergmann, D., Cameron-Smith, P., Cionni, I., Collins, W. J., Dalsøren, S. B., Doherty, R. M., Eyring, V., Faluvegi, G., Horowitz, L. W., Josse, B., Lee, Y. H., MacKenzie, I. A., Nagashima, T., Plummer, D. A., Righi, M., Rumbold, S. T., Skeie, R. B., Shindell, D. T., Strode, S. A., Sudo, K., Szopa, S., and Zeng, G.: Pre-industrial to end 21st century projections of tropospheric ozone from the Atmospheric Chemistry and Climate Model Intercomparison Project (ACCMIP), Atmos. Chem. Phys., in review, 2012a.

Young, P. J., Rosenlof, K. H., Solomon, S., Sherwood, S. C., Fu, Q., and Lamarque, J.-F.: Changes in stratospheric temperatures and their implications for changes in the Brewer–Dobson circulation, 1979–2005, J. Climate, 25, 1759–1772, doi:10.1175/2011JCLI4048.1, 2012b.

Zeng, G. and Pyle, J. A.: Changes in tropospheric ozone between 2000 and 2100 modeled in a chemistry-climate model, Geophys. Res. Lett., 30, 1392, doi:10.1029/2002GL016708, 2003.

Zeng, G., Morgenstern, O., Braesicke, P., and Pyle, J. A.: Impact of stratospheric ozone recovery on tropospheric ozone and its budget, Geophys. Res. Lett., 37, L09805, doi:10.1029/2010GL042812, 2010.

Zhong, W., Osprey, S. M., Gray, L. J., and Haigh, J. D.: Influence of the prescribed solar spectrum on calculations of atmospheric temperature, Geophys. Res. Lett., 35, L22813, doi:10.1029/2008GL035993, 2008.

ACPD
12, 26047–26097, 2012

Table 1. Models and experiment run lengths (in years). All models ran with emissions for the 1850s and 2000s; the years specified correspond to the years specified for the climate (SST/SIC).

Model	Experiments (as used in this paper) 1850s[a]	2000s[b]	Attrib[c]	ΔClim[d]	Future[e]
A. CESM-CAM-superfast	10	10	–	10	YnYY
B. CICERO-OsloCTM2	1 (2006)	1 (2006)	1	–	YYnY
C. CMAM	10 (1860s)	10 (2010s)	–	–	nYnY
D. EMAC	10	10	–	–	nYnY
E. GEOSCCM	10 (1870s)	14 (1996–)	–	–	nnnn
F. GFDL-AM3	10 (1860s)	10	–	10	YYYY
G. GISS-E2-R[f]	10 (x5)	10 (x5)	–	40	YYYY
H. GISS-E2-R-TOMAS	10	10	–	10	nnnn
I. HadGEM2	10 (1860s)	10	–	10	YYnY
J. HadGEM2-ExtTC	10 (2000s)	10	10	–	nnnn
K. LMDzORINCA	10	5 (1996–)	–	–	YYYY
L. MIROC-CHEM	11 (1850–)	11 (2000–)	–	5 (1850–)	YnYY
M. MOCAGE	4 (1850–)	4 (2000–)	–	4 (1850–)	YnYY
N. NCAR-CAM3.5	8 (1852–)	8 (2002–)	8	8 (1852–)	YYYY
O. STOC-HadAM3	10	10	10	10	YnnY
P. UM-CAM	10	10 (1996–)	10	10	YYnY
Q. TM5	1 (2006)	1 (2006)	1	–	nnnn

[a] Where models did not run 1850–1859 or 1851–1860, the climate model decade ran is indicated. Where other than 10 yr were ran, the starting year is shown.

[b] Where models did not run 2000–2009 or 2001–2010, the climate model years ran are indicated. Where other than 10 yr were ran, the starting year is shown.

[c] Details of the attribution experiments are given in Sect. 3.1.2.

[d] Details of the climate experiments are given in Sect. 3.1.3.

[e] The code shown corresponds to the four future scenarios (RCP2.6, RCP4.5, RCP6.0 and RCP8.0, in order). "Y" indicates that the scenario was run, "n" indicates that it was not.

[f] Model G ran five ensembles of the 1850s and 2000s experiments, and an average of the five ensembles is used.

ACPD
12, 26047–26097, 2012

Table 2. Natural emissions (lightning NO_x, biogenic isoprene, soil NO_x) in 1850s and 2000s. Two models (C and I) that did not include isoprene in their chemical schemes included surrogate emissions of CO. Some values are not available (n/a); where values are not available, but models ran with constant present-day (PD) values, this is indicated.

Model	Lightning NO_x $TgN\,yr^{-1}$		Isoprene $Tg\,yr^{-1}$		Soil NO_x $TgN\,yr^{-1}$	
	1850s	2000s	1850s	2000s	1850s	2000s
A. CESM-CAM-superfast	3.8	4.2	500	500	Constant PD	Constant PD
B. CICERO-OsloCTM2	5.0	5.0	449	449	8.0	8.0
C. CMAM	4.5	3.8	250 $Tg\,yr^{-1}$ CO	250 $Tg\,yr^{-1}$ CO	8.7	9.3
D. EMAC	5.3	5.7	560	591	5.8	6.0
E. GEOSCCM	5.0	5.0	411	470	6.9	7.2
F. GFDL-AM3	4.5	4.4	565	565	3.6	3.6
G. GISS-E2-R	7.5	7.7	549	602	2.7	2.7
H. GISS-E2-R-TOMAS	7.5	7.7	549	602	2.7	2.7
I. HadGEM2	1.2	1.2	475 $Tg\,yr^{-1}$ CO	475 $Tg\,yr^{-1}$ CO	5.6	5.6
J. HadGEM2-ExtTC	6.4	6.4	656	521	5.6	5.6
K. LMDzORINCA	n/a	n/a	Constant PD	Constant PD	Constant PD	Constant PD
L. MIROC-CHEM	9.3	9.7	Constant PD	Constant PD	Constant PD	Constant PD
M. MOCAGE	5.0	5.2	568	568	4.5	4.5
N. NCAR-CAM3.5	3.7	4.1	483	483	n/a	n/a
O. STOC-HadAM3	6.9	7.2	608	653	5.6	5.6
P. UM-CAM	4.9	5.1	390	390	7.0	7.0
Q. TM5	5.5	5.5	524	524	5.0	5.0

ACPD
12, 26047–26097, 2012

Table 3. Changes in tropospheric column ozone (DU) and radiative forcing ($mW\,m^{-2}$) for two different tropopause definitions (MASKZMT and MASK150). The mean and standard deviation (SD) excludes Model J.

Model	Tropospheric column O_3 change (2000s–1850s) (DU)		Tropospheric O_3 radiative forcing ($mW\,m^{-2}$)	
	MASKZMT	MASK150	MASKZMT	MASK150
A. CESM-CAM-superfast	9.4	10.0	428	446
B. CICERO-OsloCTM2	8.7	9.3	383	401
C. CMAM	7.2	7.6	315	322
D. EMAC	9.8	10.8	429	460
E. GEOSCCM	8.0	8.7	364	387
F. GFDL-AM3	9.7	10.3	406	423
G. GISS-E2-R	7.9	8.3	286	314
H. GISS-E2-R-TOMAS	8.4	8.7	305	333
I. HadGEM2	7.2	7.3	301	303
J. HadGEM2-ExtTC	8.2	8.4	315	n/a
K. LMDzORINCA	7.9	8.2	344	351
L. MIROC-CHEM	8.4	9.2	376	402
M. MOCAGE	4.7	4.8	210	219
N. NCAR-CAM3.5	9.3	10.2	406	433
O. STOC-HadAM3	9.4	10.5	396	437
P. UM-CAM	8.5	8.7	371	376
Q. TM5	9.3	10.0	399	422
Mean ± SD	8.4 ± 1.3	8.9 ± 1.5	357 ± 60	377 ± 65

ACPD
12, 26047–26097, 2012

Table 4. Influence of stratospheric adjustment and clouds (% change in ozone RFs when included) in the Edwards-Slingo (E-S) and Oslo schemes. First two rows are for all models: values are means and standard deviations. Lower rows are just for model B.

Radiation scheme	Models	Tropopause mask	Influence of stratospheric adjustment (%)			Influence of clouds (%)		
			SW	LW	net	SW	LW	net
E-S	all	MASKZMT	0	-24 ± 1	-20 ± 1	20 ± 4	-16 ± 1	-12 ± 1
E-S	all	MASK150	0	-26 ± 1	-22 ± 1	21 ± 5	-16 ± 1	-12 ± 1
E-S	B	MASKZMT	0	−25	−21	21	−17	−12
E-S	B	MASK150	0	−27	−22	22	−16	−12
Oslo	B	MASK150	–	–	–	35	−30	−22
Oslo	B	MASKOslo[a]	0	−21	−17	–	–	–

[a] Results using the Oslo model tropopause.

ACPD
12, 26047–26097, 2012

Table 5. Comparison of ozone RFs from different radiation schemes for both the clear-sky, instantaneous case, and cloudy-sky, stratospherically adjusted case. Results are shown for model B alone (to allow direct comparison of E-S and Oslo schemes), 11 models (ACE-FGIKLMNP; to allow direct comparison of E-S and NCAR schemes), and all models (for context).

		Tropopause mask	Clear-sky, instantaneous O_3 RF ($mW m^{-2}$)			Cloudy-sky, stratospherically adjusted O_3 RF ($mW m^{-2}$)		
			SW	LW	net	SW	LW	net
E-S (B)	MASKZMT	62	491	552	75	309	384	
E-S (B)	MASK150	64	521	585	78	322	401	
Oslo (B)	MASK150	72	488	560	97	264	361	
Oslo (B)	MASKOslo[a]	70	470	540	94	259	353	
E-S (11)	MASKZMT	58 ± 9	437 ± 87	495 ± 96	70 ± 13	277 ± 51	347 ± 64	
E-S (11)	MASK150	58 ± 9	463 ± 93	521 ± 101	71 ± 12	291 ± 56	361 ± 68	
NCAR(11)	MASK150	–	–	–	83 ± 16	243 ± 88	326 ± 100	
E-S (all)	MASKZMT	60 ± 9	452 ± 82	512 ± 90	72 ± 12	286 ± 49	358 ± 60	
E-S (all)	MASK150	61 ± 8	483 ± 89	543 ± 96	74 ± 12	303 ± 54	377 ± 65	

[a] Results using the Oslo model tropopause.

ACPD
12, 26047–26097, 2012

Table 6. Attribution experiments.

Attribution experiment	Climate	$[CH_4]$	Anthropogenic Emissions		
			NO_x	CO	NMVOC
#0 Em1850$CH_4$1850[a]	2000s	1850s	1850s	1850s	1850s
#1 Em2000$CH_4$2000[b]	2000s	2000s	2000s	2000s	2000s
#2 Em2000$CH_4$1850	2000s	1850s	2000s	2000s	2000s
#3 Em2000NO_x1850	2000s	2000s	1850s	2000s	2000s
#4 Em2000CO1850	2000s	2000s	2000s	1850s	2000s
#5 Em2000NMVOC1850	2000s	2000s	2000s	2000s	1850s

[a] Experiment Em1850$CH_4$1850 is the same as the core 1850s experiment for models B, J, Q.
[b] Experiment Em2000$CH_4$2000 is the same as the core 2000s experiment for all models.

ACPD
12, 26047–26097, 2012

Table 7. Methane lifetimes (yr, for the whole atmosphere), from attribution experiments, and corresponding equilibrium methane concentrations (ppbv), calculated using Eq. (1), for experiments #2–5. For experiments #0 and #1, we show observed imposed methane values.

	#0 1850s		#1 2000s		#2 1850CH_4		#3 1850NO_x		#4 1850CO		#5 1850NMVOC	
Model	τ	$[CH_4]$	τ	$[CH_4]$	τ	$[CH_4]_{eq}$	τ	$[CH_4]_{eq}$	τ	$[CH_4]_{eq}$	τ	$[CH_4]_{eq}$
B	8.06	791	8.70	1751	7.31	1384	11.60	2581	8.14	1599	8.61	1725
J	9.02	791	9.29	1751	7.80	1384	12.02	2479	8.70	1603	9.29	1752
N	9.26	791	8.11	1751	6.62	1330	12.06	2989	7.49	1571	7.82	1665
O	8.47	791	8.06	1751	6.76	1382	10.84	2612	7.68	1641	7.99	1733
P	12.29	791	11.61	1751	9.99	1428	16.38	2786	10.75	1577	11.09	1646
Q	8.55	791	8.66	1751	7.13	1349	13.15	3080	8.01	1577	8.16	1618

ACPD
12, 26047–26097, 2012

Table 8. Tropospheric ozone and methane radiative forcings ($mW\,m^{-2}$) for each model and attribution experiments #2–5 relative to experiment #1 (year 2000s). For methane radiative forcings, an equilibrium [CH_4] is calculated based on the diagnosed perturbation to the methane lifetime (Table 4); the RF is then calculated from the difference between the prescribed and equilibrium methane concentrations. For the methane experiment, also shown is the methane RF due to the prescribed (observed) 1850s–2000s change (upper box: 427 $mW\,m^{-2}$; the same in each case) and the net methane RF (lower box). For ozone radiative forcings, three numbers are given: the uppermost is the RF from the calculated ozone field (e.g. Fig. S7); the middle value is the inferred ozone RF associated with the methane adjustment to equilibrium; the lower number is the net ozone RF.

	#2. 1850CH_4		#3. 1850NO_x		#4. 1850CO		#5. 1850NMVOC	
Model	O_3 RF	CH_4 RF	O_3 RF	CH_4 RF	O_3 RF	CH_4 RF	O_3 RF	CH_4 RF
	153	427	193		38		37	
B	59	144	−132	−276	24	58	4	10
	212	571	61		62		41	
	103	427	178		29		29	
J	39	144	−78	−245	16	56	0	0
	142	571	100		45		29	
	168	427	253		48		15	
N	74	167	−217	−395	31	68	15	32
	242	594	36		79		30	
	153	427	205		36		42	
O	59	145	−137	−286	18	41	3	7
	212	572	68		54		45	
	85	427	246		35		38	
P	29	126	−92	−337	15	66	9	39
	114	553	154		50		47	
	155	427	252		45		6	
Q	65	159	−215	−420	28	66	21	50
	220	586	37		73		27	
	136	427	221		39		28	
Mean BJNOPQ	54	147	−145	−327	22	59	9	23
	190	574	76		61		37	

ACPD
12, 26047–26097, 2012

Table 9. Emission-based RFs (for 1850s–2000s) (via changes in CO_2, CH_4 and tropospheric ozone) for emitted CH_4, NO_x, CO, NMVOC, based on the mean response of the 6 models that conducted the attribution experiments (cf. IPCC-AR4 Table 2.13).

		Radiative forcing ($mW\,m^{-2}$) via:		
Emission	CO_2	CH_4	O_3	$CO_2 + CH_4 + O_3$
CH_4	18	574 (427 + 147)[a]	190	782
NO_x		−327 (−229)[b]	76 (119)[b]	−251 (−110)[b]
CO	87	59	61	207
NMVOC	33	23	37	93
Total:	138	329 (427)[b]	364 (407)[b]	831 (972)[b]

[a] The methane RF is shown as the direct RF (due to the increase in CH_4 concentration: $427\,mW\,m^{-2}$) and the component from the change in methane lifetime.

[b] The values in brackets apply a crude correction to the NO_x components to force the CH_4 RF to match the observed value (see text for details).

ACPD
12, 26047–26097, 2012

Table 10. Tropospheric ozone RFs ($mW\,m^{-2}$) relative to the 1850s (for MASKZMT) (also see Fig. 7.).

Model	1980s	2000s	RCP2.6 2030s	RCP2.6 2100s	RCP4.5 2030s	RCP4.5 2100s	RCP6.0 2030s	RCP6.0 2100s	RCP8.5 2030s	RCP8.5 2100s
A	364	428	329[a]	150[a]	–	–	364[a]	229[a]	521	733
B	307	384	345	164	406	262	–	–	456	527
C	262	315	–	–	341	202	–	–	385	490
D	337	429	–	–	439	308	–	–	–	680
E	312	365	–	–	–	–	–	–	–	–
F	365	407	367	195	443	328	439	335	513	775
G	275	297	293	184	330	235	325	301	420	567
H	271	311	–	–	–	–	–	–	–	–
I	227	302	–	150	–	270	–	–	–	570
J	–	316	–	–	–	–	–	–	–	–
K	279	345	280	123	355	237	307	227	391	484
L	302	377	323	177	–	–	367	260	441	527
M	190	211	191	106	–	–	222	157	309	430
N	337	406	338	156	402	261	353	230	449	587
O	336	396	339	154	–	–	–	–	468	560
P	296	371	367	253	427	356	–	–	474	637
Q	–	399	–	–	–	–	–	–	–	–
Mean ± SD (all)	297 ± 49	356 ± 58	317 ± 52	165 ± 39	393 ± 45	273 ± 49	340 ± 66	249 ± 58	439 ± 61	582 ± 100
Mean ± SD (FGKN)	314 ± 44	364 ± 53	320 ± 40	165 ± 32	382 ± 50	265 ± 43	356 ± 58	273 ± 53	443 ± 52	603 ± 123
Mean ± SD (ABFGKLMNOP)	305 ± 51	362 ± 65	317 ± 52	166 ± 40	–	–	–	–	444 ± 62	583 ± 107

[a] Model A (CESM-CAM-superfast) RCP2.6 and 6.0 results used SST/SIC inconsistent with these scenarios.

ACPD
12, 26047–26097, 2012

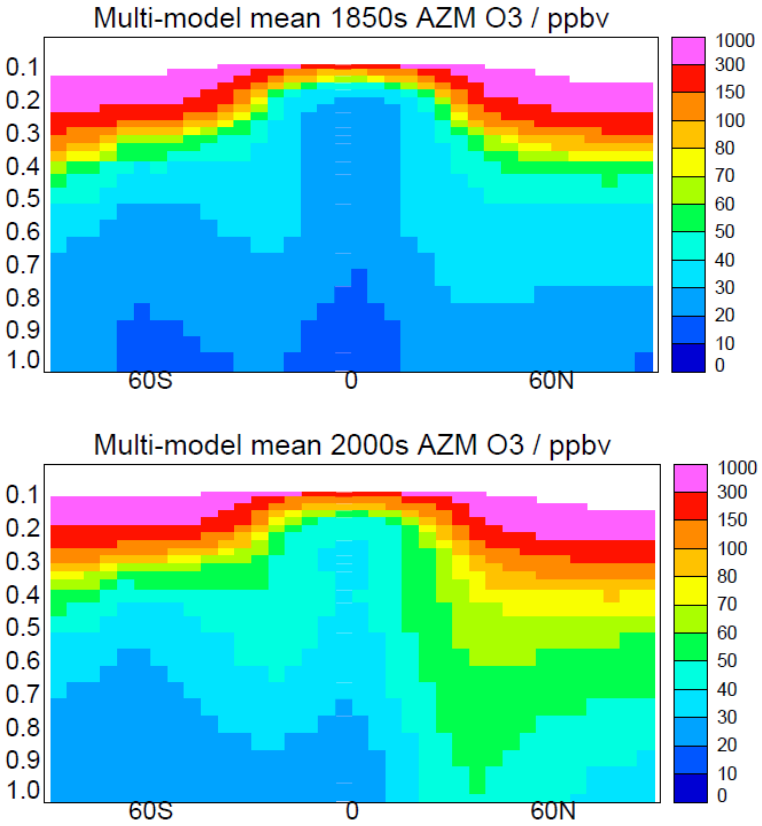

Fig. 1. Multi-model mean annual zonal mean ozone (ppbv), for the 1850s and 2000s. Vertical grid is hybrid – all models have been interpolated to a common grid. Figure S1 (Supplement) shows equivalent plots for all models.

ACPD
12, 26047–26097, 2012

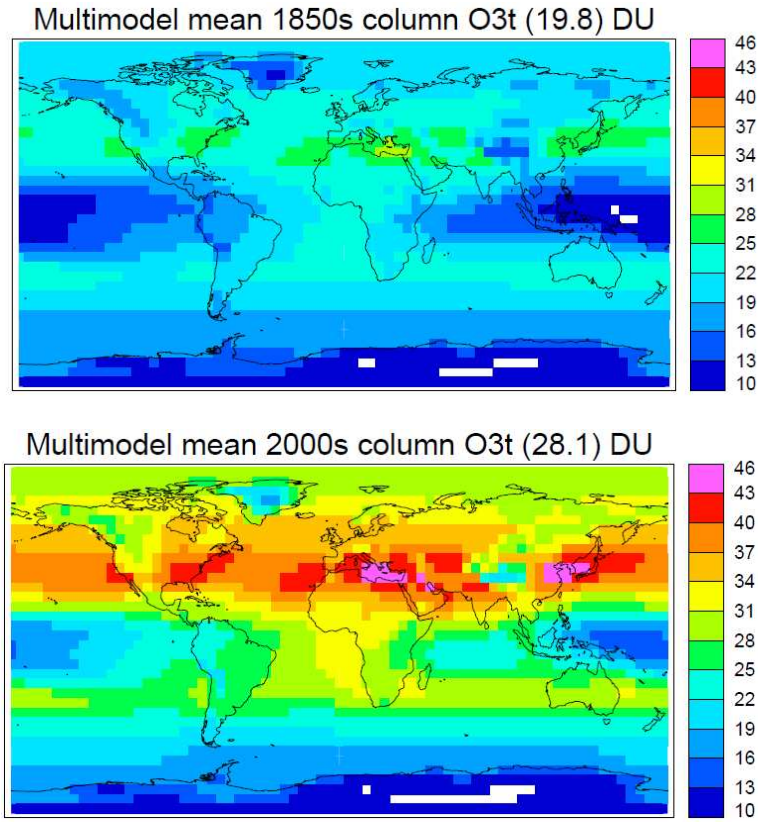

Fig. 2. Multi-model mean annual mean tropospheric column ozone (DU), for the 1850s and 2000s (for MASKZMT). Area-weighted global mean values are in brackets. Figure S2 (Supplement) shows equivalent plots for all models.

ACPD
12, 26047–26097, 2012

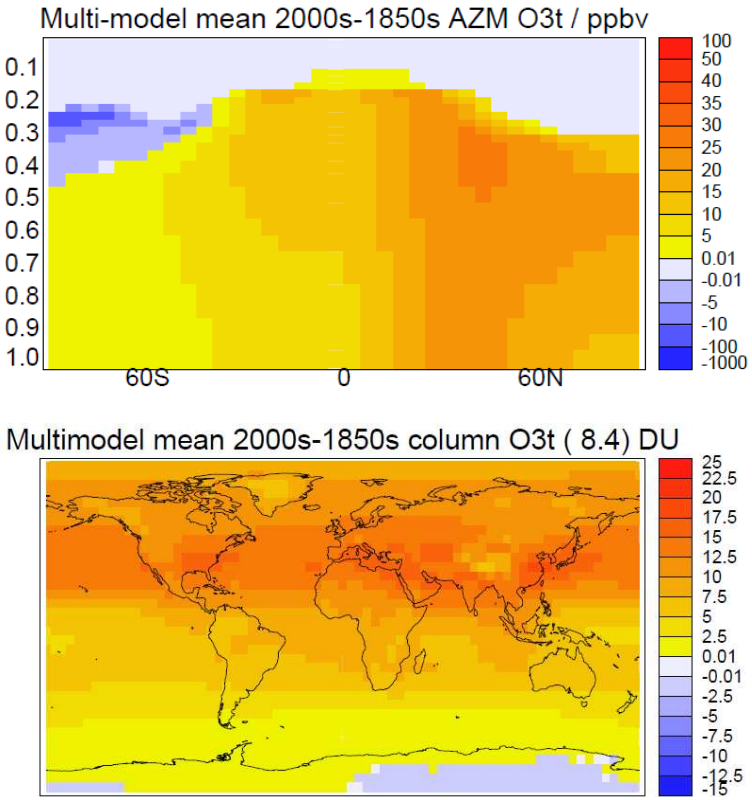

Fig. 3. Multi-model mean changes (2000s-1850s) in: **(a)** annual zonal mean ozone (ppbv) (masked at tropopause); **(b)** tropospheric column ozone (DU). Tropopause is a climatological monthly zonal mean (MASKZMT), as used by Cionni et al. (2011). Figure S3 (Supplement) shows equivalent plots for all models.

ACPD
12, 26047–26097, 2012

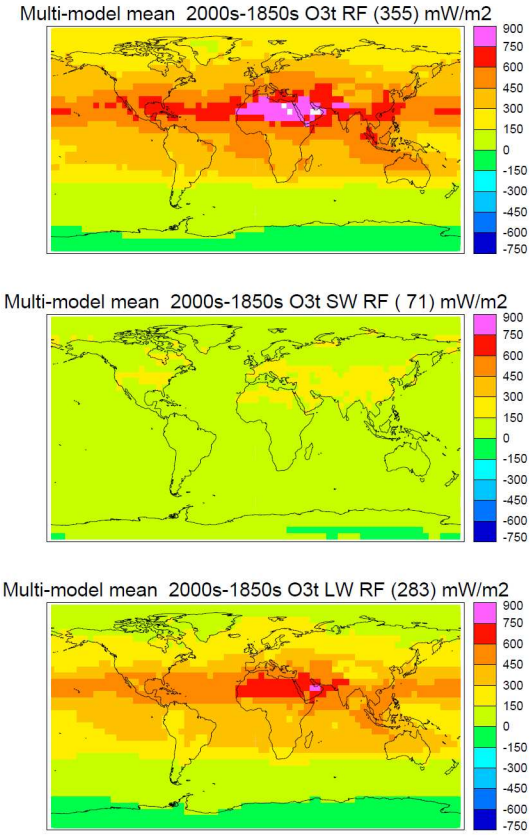

Fig. 4. Multi-model mean annual mean tropospheric ozone total, shortwave (SW; solar wavelengths), and longwave (LW; infrared wavelengths) radiative forcings ($mW\,m^{-2}$), between the 1850s and 2000s (for MASKZMT). Area-weighted global mean values are in brackets. Figure S4 (Supplement) shows equivalent plots for all models.

ACPD
12, 26047–26097, 2012

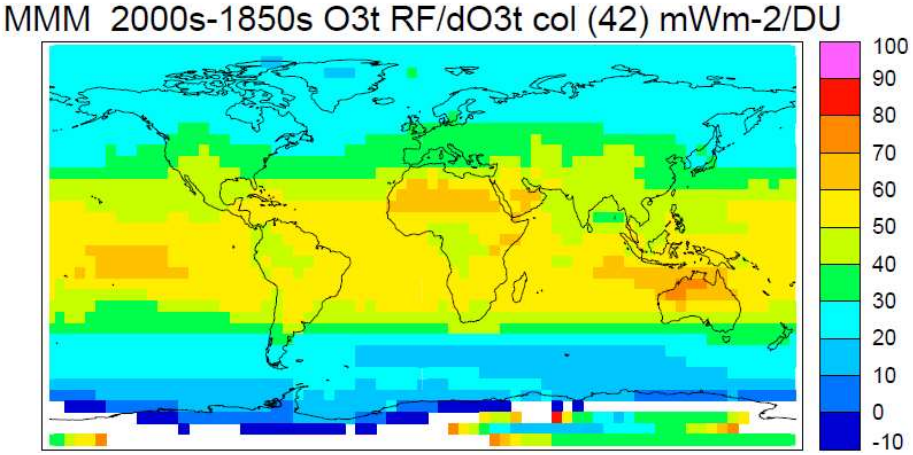

Fig. 5. Multi-model mean normalised ozone radiative forcing ($mW\,m^{-2}\,DU^{-1}$) (for MASKZMT). Area-weighted global mean value is in brackets. Figure S5 (Supplement) shows equivalent plots for all models.

ACPD
12, 26047–26097, 2012

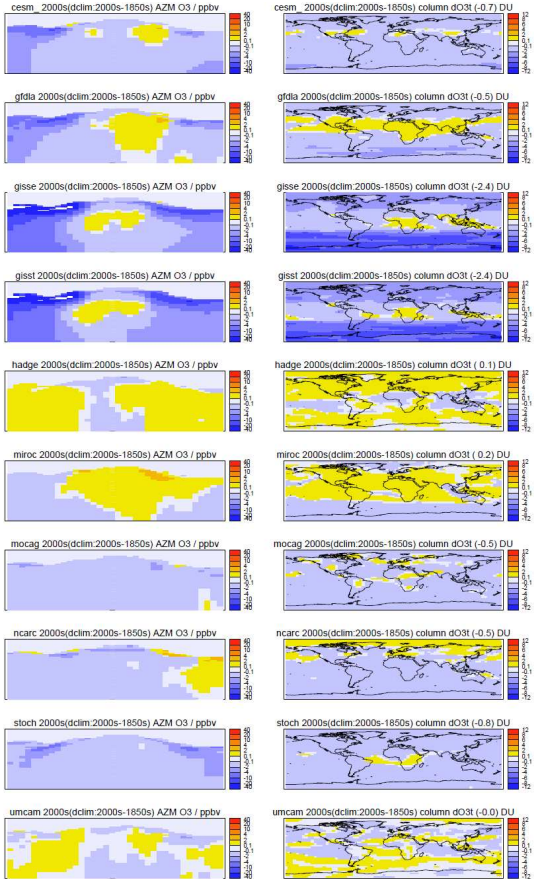

Fig. 6. Response of ozone to climate change (2000s emissions; 2000s climate – 1850s climate) in ten models. Left hand column are annual zonal mean changes (ppbv); right hand column are annual tropospheric column ozone changes (DU; global mean value in brackets; for MASKZMT).

ACPD
12, 26047–26097, 2012

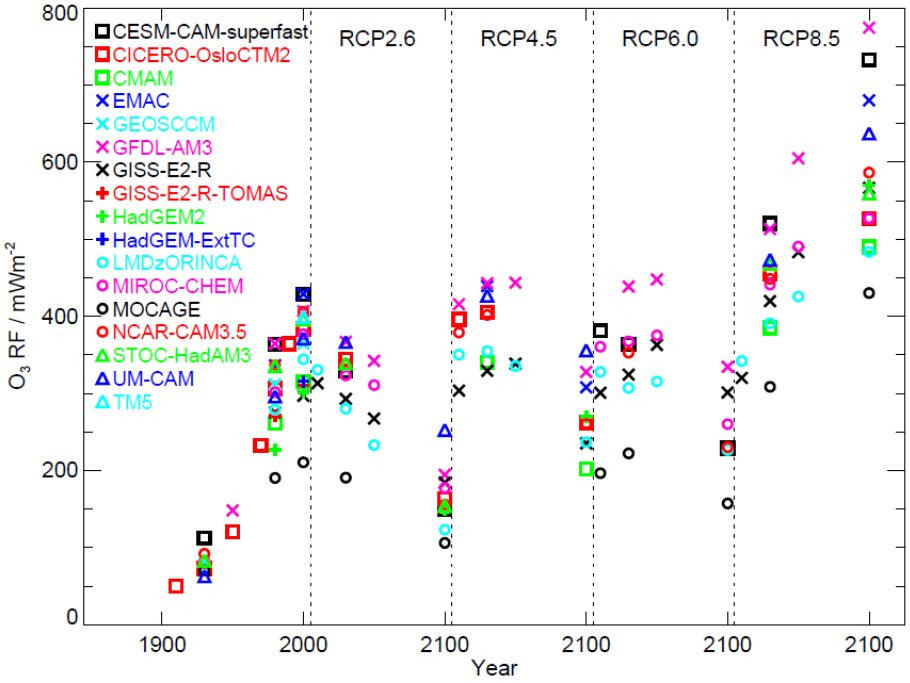

Fig. 7. Tropospheric ozone radiative forcing ($mW\,m^{-2}$) relative to 1850s, for all available models and timeslice experiments (1910s, 1930s, 1950s, 1970s, 1980s, 1990s, 2000s; then for the four future RCP scenarios 2010s, 2030s, 2050s and 2100s). All models ran the 2000s and 1850s; for other timeslices, varying subsets of models are available. RF values were calculated using MASKZMT.
[a]Model A (CESM-CAM-superfast) RCP2.6 and 6.0 results used SST/SIC inconsistent with these scenarios.

ACPD
12, 26047–26097, 2012